The influence of cationic substitution on the magnetic properties of cobalt ludwigite

Yuriy V. Knyazev

Siberian Federal University 2017

ABSTRACT

This thesis explores oxyborate samples substituted by a series of transition cations. These materials represent a wide class of strongly correlated oxide systems that demonstrate effects of magnetic frustrations, charge ordering and multistage magnetic transitions. These lead to a number of unusual magnetic phenomena. Oxyborates show a rich spectrum of magnetic states (spin glass, random magnetic chains, quantum entanglement, two-dimensional Sastri-Sutherland lattice, long-range magnetic order). In this work, we consider an interesting orthorhombic oxyborates of the ludwigite structural type: $Fe_3O_2BO_3$, $Co_3O_2BO_3$, $Co_{2.25}Fe_{0.75}O_2BO_3$, $Co_{2.88}Cu_{0.12}O_2BO_3$ and $Co_{1.7}Mn_{1.3}O_2BO_3$. The crystal structure of ludwigites is represented by zigzag-like walls formed by oxygen octahedra with metallic ions inside. Magnetic ions form a distorted triangular structure. Thus, magnetic ions form a three-dimensional framework of exchange bonds. Geometric factors associated with the crystal structure lead to a situation where the interactions between magnetic nearest neighbors along one of the crystallographic directions are substantially weakened, in comparison with interactions in other directions. Therefore, the experimental observation of quasi-low-dimensional magnetic behavior in ludwigites is possible. The chains of magnetic ions belonging to one crystallographic position are actually equivalent to one-dimensional chains. Three chains are combined to form quasi-two-dimensional three-pillar spin stairs (*Three spin-leg ladders, 3LL*). In this study, the considered samples are characterized by magnetic and Mössbauer measurements, X-ray diffraction and theoretical calculations of indirect exchange interactions. The effect of substitution on anisotropic properties has also been studied.

We studied the crystal structure of $Co_{2,25}Fe_{0,75}O_2BO_3$, $Co_{2,88}Cu_{0,12}O_2BO_3$, and $Co_{1,7}Mn_{1,3}O_2BO_3$ single crystals by X-ray diffraction. It allowed us to define structural parameters and analyze the cation distribution by position, as well as the effect of cation substitution on structural parameters. The distribution of Fe ions over non-equivalent positions, as well as a charge and magnetic states were measured by

Mössbauer spectroscopy on the $Co_{2,25}Fe_{0,75}O_2BO_3$. Mössbauer spectroscopy also measured the temperature of magnetic ordering in this compound.

We obtained the field, temperature and angular dependences of the static magnetization and the dynamic magnetic susceptibility for all series of the ludwigite single crystals. Using magnetic data, the magnetic characteristic, such as the temperature of the magnetic ordering, magnetic moments were calculated. Investigations of the effect of cation substitution on the magnetic properties of $Co_{2,25}Fe_{0,75}O_2BO_3$, $Co_{2,88}Cu_{0,12}O_2BO_3$, and $Co_{1,7}Mn_{1,3}O_2BO_3$ samples were carried out. We have calculated integrals of indirect exchange interactions in the framework of the indirect exchange coupling model. Using this model, the effect of cation substitution on the magnitude and sign of the integrals of indirect exchange interactions and the role of frustrating exchange interactions in the formation of the magnetic state of cobalt ludwigites were studied.

LIST OF THE ARTICLES PUBLISHED

1 N.B. Ivanova, N.V. Kazak, Yu.V. Knyazev et al. Structure and magnetism of copper substituted cobalt ludwigite $Co_3O_2BO_3$// Low Temperature Physics. – 2013. – Vol. 39(8). – P. 913 – 917.

2 Yu.V. Knyazev, N.B. Ivanova, N.V. Kazak, et al. Crystal structure and magnetic properties of Mn substituted ludwigite $Co_3O_2BO_3$. //Journal of magnetism and magnetic materials. – 2012. – Vol. 324. – P. 923 – 927.

3 J. Bartolomé, A. Arauzo, N. V. Kazak, N. B. Ivanova, S. G. Ovchinnikov, Yu. V. Knyazev and I. S. Lubutin. Uniaxial magnetic anisotropy in-$Co_{2,25}Fe_{0,75}O_2BO_3$compared to $Co_3O_2BO_3$ and Fe_3O_2BO ludwigites. //Physical Review. B. – 2011.– Vol.83. – P.144426 (1-12).

4 N. V. Kazak, N. B. Ivanova, O. A. Bayukov, S. G. Ovchinnokov, A. D. Vasiliev, V. V. Rudenko, J. Bartolome, A. Arauso, Yu. V. Knyazev.The superexchange interactions in mixed Co-Fe ludwigite. //Journal of magnetism and magnetic materials. – 2011. – Vol. 323. – P. 521-527.

TABLE OF CONTENTS

LUDWIGITES PHYSICAL PROPERTIES REVIEW

1.1 Crystal structure.

The oxyborates with the ludwigite structure have the general formula $M_2^{2+}M^{3+}O_2BO_3$[1,2]. The title of these materials dates back to the Austrian professor Ernst Ludwig, who first discovered the natural mineral ((Mg,Fe) $^{2+}{}_2Fe^{3+}[BO_3]O_2$ [3,4,5]. To date, many artificially synthesized compositions with ludwigite structure exist. This structure predicts that the ions of Co^{2+}, $Ni^{2+}$and Mg^{2+} usually have a divalent valence state. The trivalent ion can be represented by magnetic Ti^{3+}, Cr^{3+}, Mn^{3+}, Fe^{3+}, Co^{3+}[6-10], as well as nonmagnetic ions, Ga^{3+}, Al^{3+}[11, 12]. In the case of the isomorphous substitution of $2M^{3+} \rightarrow (M^{2+} + M^{4+})$, ions Mg^{2+} and Sn^{4+}, In^{4+}, Ge^{4+}, Ti^{4+}, etc. can appear as a pair of M^{2+} and M^{4+} ions [13-16]. The majority of samples are heterometallic compounds that contain cations of different chemical elements ($M^{2+} \neq M^{3+}$). Up to date, only two homometallic compounds are known. They are $Co_3O_2BO_3$ and $Fe_3O_2BO_3$.

The crystalline structure of ludwigites refers to the orthorhombic system (the spatial group of *Pbam* [17]). However, copper-based ludwigites which have Jahn-Teller Cu-ion, have decreasing symmetry to the monoclinic ($P2_1/c$) [6]. The unit cell of ludwigite contains $Z = 4$ formula units with cell parameters of a ≈ 9 Å, b ≈ 12 Å, c ≈ 3 Å. Metal ions occupy four nonequivalent crystallographic positions 2a, 2d, 4g and 4h according to the symbolism of Wyckoff [18]. In the literature on nonequivalent positions, the following notation is accepted: 2a -1, 2d -2, 4g -3 and 4h-4. Boron occupies one position, and oxygen is located in five nonequivalent sites. Oxygen atoms form the octahedral environment with the metal ions in it. Oxygen octahedrons are combined into zigzag walls through the common edge. As shown by electron microscopy, these walls propagate along the *c*-axis [19, 20] and form a three-dimensional crystalline structure through a common oxygen atom and planar BO_3-groups.

In the ludwigite structure, the metal-to-metal distances are in the range of 2.8-3.4 Å. Magnetic ions are located at the vertices of the triangles. Two types of interionic distances can be distinguished in the ludwigite structure: $d_{max} = d_{13} \approx 3.4$ Å and $d_{min} = d_{24} \approx 2.8$ Å, which corresponds to the largest and shortest metal-to-metal distance. Triads of magnetic ions in positions 4-2-4 and 3-1-3 form quasi-two-dimensional three-legged spin ladders (*Three Leg Ladders, 3LL*) [21]. As will be shown below, the inter- and intra-ladders exchange interactions play an important role in establishing the main magnetic state in the ludwigites.

Metal ions can randomly occupy non-equivalent positions, which leads to the appearance of cationic disorder and allows us to consider ludwigites as disordered systems. Cationic disorder is typical for heterometallic samples and can lead to the loss of long-range magnetic order (spin-glass state) [11] and electronic properties (the appearance of hopping conductivity of the VRH type) [32].

As mentioned previously, the ludwigite structure is characterized by the presence of metal ions with different valences (M^{2+}, M^{3+}). Therefore, the valence state determination of each cation is most relevant. The empirical method of bond valence sum (BVS-method) based on the second Pauling rule could be used [22-24]. According to this method, the valence of the ion at the site (V) is determined by the sum of the valences of all bonds with the nearest ions (S_{ij}). Calculations clearly show that position four is occupied by trivalent ions, while other positions 1, 2 and 3 are occupied by divalent ions.

1.2 Magnetic properties

A variety of physic of magnetic phenomena in ludwigites led to an extreme interest in the precise study of these materials. Ludwigites represent a class of magnetic materials with frustrated exchange interactions and exhibit a rich spectrum of magnetic states (random spin chains, spin ladders, long-range magnetic order and spin-glass state). The transition of long-range magnetic order (antiferromagnetism, ferrimagnetism) to short-range magnetic order (spin-glass) can be caused by cation-

ic substitution, as was observed, for example, for $Fe^{2+}{}_2Fe^{3+}O_2BO_3 \rightarrow Mg^{2+}{}_2Fe^{3+}O_2BO_3$ [35].

Large negative values of the Curie-Weiss temperature (| θ | = 100-500 K) indicate the dominant role of antiferromagnetic interactions in the ludwigite. The triangular arrangement of magnetic ions and strong antiferromagnetic interactions allows for the frustration effects. Under frustrations in solid-state physics, we mean the impossibility of minimization of the spin Hamiltonian due to the strong completion of exchange interactions. Huge frustration level leads to degeneracy of the ground state of the system with nonzero entropy at zero temperature. In real systems frustrations can decrease the ordering temperature, i.e. the phase transition occurs at temperatures much lower than expected from the evaluation of exchange interactions ($T_{tr} << J/k_B$). Ultimately, frustrations can lead to a disordered magnetic state, including the spin-glass state. The ratio of the paramagnetic Curie temperature to the temperature of the magnetic transition is often used as a criterion for estimation of the frustrations level. For ludwigites, the typical value is $\theta/T_{tr} \approx 17$ [2, 4].

It is possible that interactions between nearest magnetic neighbors along the crystallographic direction are weakened compared to the interactions in other directions. Therefore, experimental observation of low-dimensional magnetic behavior is possible. The chains of magnetic ions belonging to one crystallographic position are equivalent to one-dimensional chains. According to the experimental data of the Mossbauer effect [25,26] and direct studies of the magnetic structure by neutron scattering [27,28], magnetic structure of the ludwigite $Fe_3O_2BO_3$ splits into two quasi-two-dimensional structures consisting of spin chains. Cations in positions 1 and 3 form a spin ladder of type I (3-1-3), cations in positions 2 and 4 - a ladder of type II 4-2-4 (see Fig.4). The study of the thermodynamic properties of $Fe_3O_2BO_3$ revealed two transition temperatures at T_{N1} = 112 K and T_{N1} = 75 K associated with magnetic phase transitions [29,30].

Mössbauer effect in Fe_3BO_5 indicates the establishment of long-range magnetic order in the triads 4-2-4 at 112 K (phase AF1) [25]. At T_{N2} = 75 K, a transition

to weak ferromagnetism occurs due to ordering within the triads 3-1-3 (phase WF). Below 50 K, the system goes over into the antiferromagnetic phase AF2. At the same time, only the low-temperature singularity at 75 K is observed by the temperature dependences of magnetization and magnetic susceptibility) [30,31]. The absence of an anomaly at 112 K stimulated the investigation of the magnetic structure of this material by neutron diffraction.

Experiments on Fe_3BO_5 were first performed by J. Attfield et al. (1992) [27], and then repeated by P. Bordet et al. (2009) [28]. In the first case, the magnetic structure was studied at 5 K, and the second - in the temperature range of 5-120 K. As a result, a two-stage ordering of the magnetic moments was revealed: at T_{N1} = 112 K for magnetic moments in the spin ladder of the 4- 2-4 in the direction of the *b* axis, at T_{N2} = 74 K for magnetic moments in the ladder 3-1-3 along the *a*-axis. The magnetic moments of Fe^{2+}ions inside the triad 3-1-3 ordered antiferromagnetically in ferromagnetic chains appear that propagate along the *c*-axis. The magnetic moments between the triads 4-2-4 are ordered antiferromagnetically along the *c*-axis, whereas the ordering in the triad 4-2-4 differs for different neutron diffraction data. Thus, according to the data [28], the mutual orientation of the magnetic moments in the triad 4-2-4 is ferromagnetic, according to another paper [27] – antiferromagnetic.

Up to date, measurements of the magnetic characteristics of $Fe_3O_2BO_3$ have been performed on polycrystalline samples and single crystals along the *c*-axis. The chosen geometry of the experiment is the reason that the high-temperature magnetic transition at 112 K did not manifest itself in magnetic measurements. Therefore, precision measurements of the magnetization along the crystallographic directions *a*, *b*, and *c* are relevant for the observation of magnetic transitions.

It was shown in [32] that $Co_3O_2BO_3$ is a ferrimagnet with the easy axis of magnetization *b*. The presence of hysteresis loops indicates a ferromagnetic ordering of magnetic moments in this direction [33]. In directions *a* and *c* an antiferromagnetic contribution is expressed. Strong magnetic anisotropy also appears in the par-

amagnetic region, where the temperature dependence of the magnetization obeys the Curie-Weiss law with the paramagnetic Curie temperatures θ_b = 1.2 K, $\theta_{a,c}$ = -153.8 K.

Studies of the oxyborate $Mg_2FeO_2BO_3$ demonstrate that a transition to the spin-glass state arises through an intermediate state and it is characterized by the formation of random spin chains with half-integer spin (S_{Fe}^{3+} = 5/2) and strong antiferromagnetic interaction along the chain [34, 35]. Short-range correlations grow as the temperature decreases. These excitations are well described in the framework of a one-dimensional Heisenberg antiferromagnet. Quasi-one-dimensional Heisenberg antiferromagnetic chains in some form are realized in $Cu_2GaO_2BO_3$ [36]. This system is a spin chain with S = ½ and strongly frustrated interactions, therefore the long-range magnetic order arises only at a temperature T_N = 3.4 K

The possibility of synthesizing ludwigites with different 3d-metal ions allows for accurate investigations of the magnetic states nature and to establish a relationship between structural features and magnetic behavior.

1.3 Theoretical approaches of the magnetic properties description

The variety of possible magnetic structures of ludwigites raises a number of questions. What is the key factor in the formation of the basic magnetic state of these materials? What role do the features of the crystal structure and cation distribution play in macroscopic magnetic behavior? The answer to these questions with the help of only experimental methods of investigation proves to be a difficult task, therefore, theoretical studies of the magnetic structure based on various techniques are increasingly being used [37-43].

Now, there are no true reasons for the huge difference in the magnetic properties of the two currently known samples of homo-metallic ludwigites$Fe_3O_2BO_3$ and Co_3BO_5. These samples with the same structure and similar atomic composition, exhibit crucially different magnetic properties. Therefore, detailed study of the causes of this difference is required.

One of the first theoretical approaches devoted to $Fe_3O_2BO_3$, Vallejo [37], considered spin ordering within 3LL. It studied the exchange of localized classical spins interacting through conduction electrons (double in a triad of 4-2-4). The paper also considered the issue of competition of double exchange and antiferromagnetic indirect exchange interactions for the determination of the magnetic phase.

The description of the magnetic structure is based on the interactions between localized Fe^{3+} spins via band electrons. To describe these interactions, the tight-binding approximation Hamiltonian with the indirect exchange interactions between the local spins was used:

$$H = -\sum_{\langle ij \rangle} (t^e_{i,j} c^+_i c_j + \text{H.c.}) + \sum_{\langle ij \rangle} J_{ij} \vec{S}_i \cdot \vec{S}_j.$$

The parameter J is a random variable with probability of distribution $P(J)$. It describes the interaction between nearest magnetic neighbors. The study of the function $P(J)$ was performed in [44]. Analysis and calculation of the Hamiltonian using the Monte Carlo method, based on the two-coordinate double exchange model, resulted in the determination of possible magnetic structures. Thus, it was shown that in addition to the ferromagnetic phase, a phase with ferromagnetically ordered moments 4-2-4, antiferromagneticor canted phase could also exist.

Theoretical predictions of the ferromagnetic order in the triad 4-2-4, which are ordered antiferromagnetically, agree with the experimental neutron diffraction data [27]. On the other hand, the existence of a skew structure contradicts the results of the Mössbauer data [25]. Below 74 K, the calculations of the magnetic structure contradict the experimental results obtained with the help of the Mössbauer and neutron diffraction data [25, 26, 28].

Elastic lattice interactions could improve the one-dimensional exchange model for three magnetic ions in the spin ladder 4-2-4, taking into account the distortion of the crystal lattice [38].

The Hamiltonian of this model is represented in the following form:

$$H = -t\sum_i (1+\delta_i)\cos\left(\frac{\theta_i}{2}\right)(c_i^+ c_{i+1} + \text{h.c.}) \quad + JS^2\sum_i \cos(\theta_i) + B\sum_i \delta_i^2 + V\left(\sum_i \delta_i\right)^2$$

Here, the first term expresses the interaction through the conduction electrons with the transfer parameters c_i, the second term is the indirect exchange interaction of magnetic ions with the coupling angle θ, and the distortions of the crystal lattice are described using the displacement parameters δ.

The calculation of this Hamiltonian has shown that a magnetoelastic effect observed in ludwigite is a result of the interaction between magnetic spins and the effect of lattice distortion. Magnetic phases, charge ordering, and lattice compression were obtained in good qualitative agreement with neutron diffraction [28] and X-ray [44] studies, respectively. Possible magnetic states were obtained in a wide range of magnetic and electron hopping energies. However, an explicit binding to temperature and exchange energy for real ludwigite $Fe_3O_2BO_3$is not considered. We also note that the authors do not consider the reasons for the appearance of two independent magnetic sublattices, which are ordered independently of each other.

Another attempt to describe the magnetic structure of ludwigite at $Fe_3O_2BO_3$ in the ground magnetic state was undertaken by calculating the density functional theory in the VASP software package [45] assuming a noncollinear arrangement of interacting spins in the crystal lattice at a temperature of 15 K. The "input" models considered the experimental spin configurations and the other variants of the arrangement of the magnetic moments in the triads 4-2-4. As a result, it was found that the spin configuration in these triads is noncollinear with the formation of ferromagnetically oriented Fe2-Fe4a dimers with a binding energy of 0.4 eV.These dimers are weakly bound to the Fe4b cation with magnetic moment angle of 78° to this dimer.

As for the second type of triad (3-1-3), an antiferromagnetic orientation in the *ab*-plane and ferromagnetic along the c axis with a binding energy on the order of

0.8 eV were obtained, which agrees qualitatively with the data of the neutron diffraction [27,28].

These approaches, however, do not fully explain the mechanism and nature of the formation of magnetic structure and do not receive the quantitative values of the interactions in an explicit form.

Since, most of synthesized ludwigites are magnetic insulators, the magnetic structure is determined primarily by indirect exchange interactions between magnetic ions. The Hamiltonian of such systems has a simpler form:

$$H = \sum_{i=1}^{L} J_i \vec{S}_i \cdot \vec{S}_{i+1},$$

here $\vec{S}_i$ is the spin operator, J_i is the integral of the indirect exchange interaction between a pair of magnetic ions.

According to this approach, the magnetic interactions are based on the Goodenough-Kanamori rules [46] and indirect exchange that is expressed by Anderson [47].We take into account the experimental parameters of the excitation of the electron of the ligand cation and integrals of intra-atomic exchange [48,49]. The model of indirect exchange coupling considers the orbital overlap cation-ligand-cation and allows us to perform accurate description of the magnetic structure. The model validity was demonstrated on spinel ferrites [50-52]. Later this method was used for ludwigite $Cu_2FeO_2BO_3$ [35].

According to this model, superexchange interactions are the most important interactions in the formation of a magnetic structure. The calculations were carried out from parameters of a solid-state crystalline structure. Let us consider an application of this model to Cu_2FeBO_5. Calculations show that this compound is an antiferromagnet with a magnetic ordering temperature of 34 K, which is very close to the experimental value of 32 K. The frustrating and ordering interactions, which describe the magnetic structure, were discriminated. Note that the calculated interactions in triads 4-2-4 are ordered for $Cu_2FeO_2BO_3$. It was also shown that strong frus-

trating bonds lead to a low value of the ordering temperature and can obviously lead to the formation of a spin-glass phase of iron ions at 63 K, as found in [6].

The indirect exchange coupling model contributes to an accurate description of the magnetic structure of ludwigites with another cationic composition, as well as highlights those interactions that seek to establish a magnetic order in the system and interactions that are hindered (frustrating). This model allows theoretical predictions of the magnetic ordering temperature with sufficient accuracy.

In this paper, the described model is used as the main tool for understanding the magnetic structure of a number of ludwigites.

2. SAMPLES AND EXPERIMENTAL TECHNIQUES

Single crystals of $Co_{3-x}Fe_xO_2BO_3$ were grown by the flux method in the system Co_3O_4–Fe_2O_3–B_2O_3–PbO–PbF_2. The relative content of Co and Fe ions in the prepared compounds was first estimated from the mass ratio of initial components $Fe_2O_3/(Fe_2O_3 + Co_3O_4)$, and was later checked by X-ray and Mössbauer measurements. At relatively high Co:Fe ratio in the solution (> 2.5) we have succeeded in preparing high quality single crystals $Co_{3-x}Fe_xO_2BO_3$ with ludwigite structure and maximal substitution *x* value near 1. All the samples had a needle shape up to 4 mm long (see Fig. 1). Sample's maximumweight was about 1.2 mg. By lowering the Co:Fe concentration ratio in the solution the tendency to the synthesis of warwickite phase appears in our synthetic process. At equal concentrations of cobalt and iron ions in the solution single crystals of warwickite structure with the lattice parameters a = 3.134(2); b = 9.269(7); c = 9.430(7) Å were grown.

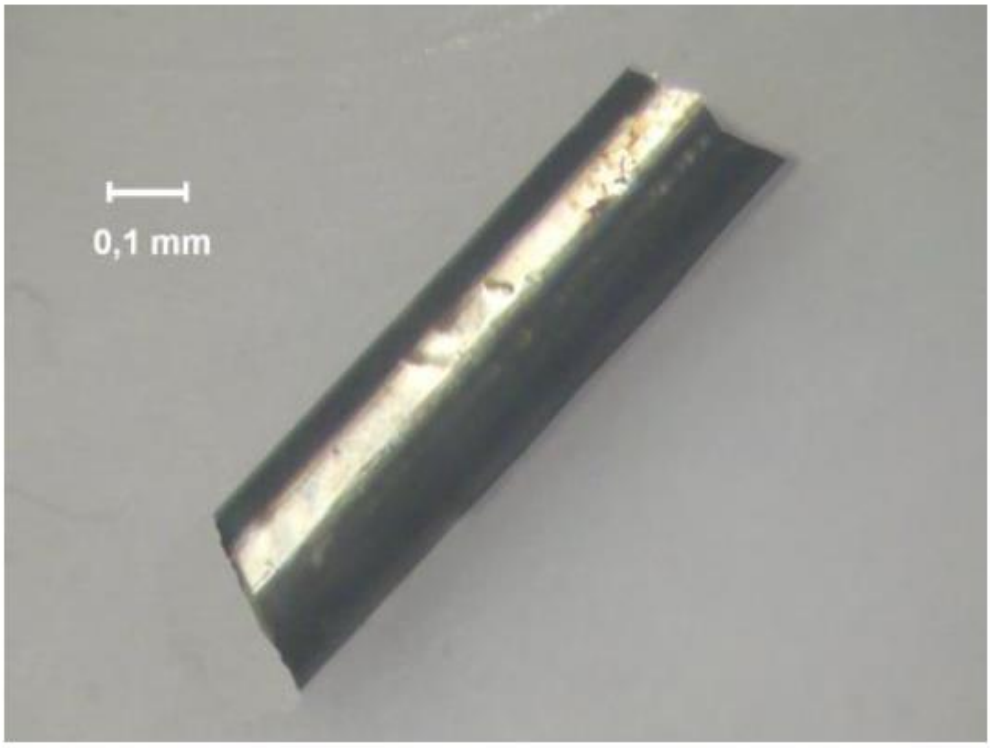

Fig. 1. Representation of high-quality ludwigite single crystals. The samples is a black needle up to 4 mm long.

The single crystals $Co_3O_2BO_3$ and $Co_{3-x}Mn_xO_2BO_3$ have been grown by the solution method. For the first compound the chemical components were taken in the next molar relation:

$Bi_2Mo_3O_{12} : B_2O_3 : CoO : Na_2O : Co_2O_3 = 3 : 1 : 2 : 2 : 2$.

Then the part of cobalt oxide Co_2O_3 was substituted by Mn_2O_3. For the total solution and homogenization, the composition was heated to 1100 ^{0}C.

Single crystals of $Co_{3-x}Cu_xO_2BO_3$ were grown by the flux method in a system Co_3O_4-CuO-B_2O_3-PbO-PbF_2. The relative amounts of Co and Cu ions in the prepared compound were later checked by X-ray diffraction. After mixing of the components, the composition was heated up to 1100 ºC and kept at this temperature for about 3 h. Then the solution was subjected to two-step cooling.

After 3 hours, the solution underwent two steps cooling. The first step: fast cooling to 930 ^{0}C. The second step: slow cooling by 12 ^{0}C a day during three days. During these three days, spontaneously formed single crystals were grown. Then the crystals were cleaned by a 20% water solution of nitric acid. The single crystals were needle shaped, up to 4mm long, and black in color, similar to their prototype $Co_3O_2BO_3$. The long side of the needle in $Co_3O_2BO_3$, $Co_{3-x}Fe_xO_2BO_3$, $Co_{3-x}Cu_xO_2BO_3$ and $Co_{3-x}Mn_xO_2BO_3$ coincides with crystallographic *c*-direction.

X-ray diffraction measurements were made on one of the single crystals and the crystallographic structure was resolved in detail. A SMART APEX II (MoKα radiation, CCD detector) X-ray diffractometer was used. The scanning angle 2θ = 5.4 - 58° (R1=1.40 %, wR2=3.31%). The Rietveld plot of the X-ray data refinement is shown in Fig. 2.The site occupation factors determined for the different transition ions in the distinct crystallographic positions were used to calculate the relative amount of 3d-elements in the material.

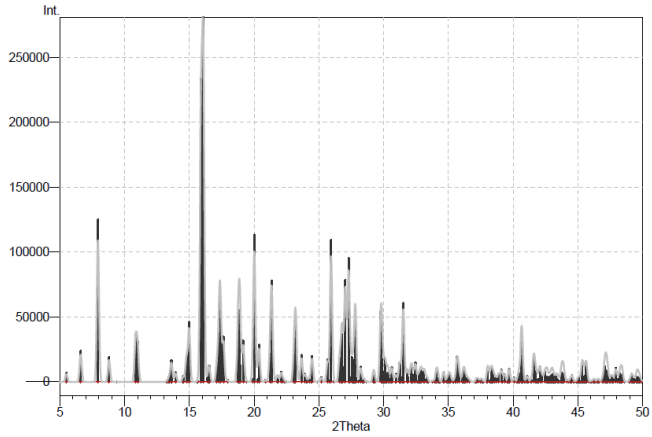

Fig. 2. Experimental (light) and calculated (dark) X-ray pattern of $Co_{2,25}Fe_{0,75}BO_5$. Calculated peaks shown by hatches.

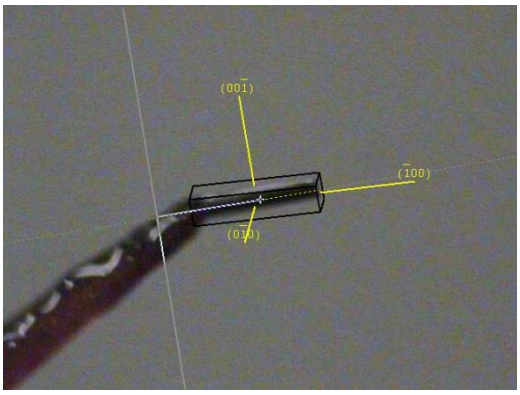

Fig. 3.X-ray diffractometer orientation of ludwigite $Co_{2,25}Fe_{0,75}BO_5$.

The Mössbauer spectrometer used a Co^{57}(Cr) source and operated in the regime of constant acceleration with powder samples that have relative natural Fe-density towards to 5-10 mg/cm^2. The isomer shift value was determined with reference to metallic α-Fe. The spectrum interpretation were carried out in two stages. At the first stage, the probability distribution of quadrupole splittings P(QS) was determined. The peculiarities in this distribution testify that there are possible nonequivalent positions (sites) of the iron. The probability distribution gives only qualitative information, since, when fitting, we used one value of the isomer shift common to a group of the doublets. This information was used to construct a model spectrum. At the second stage, the model spectrum was fitted to the experimental spectrum by varying the overall set of hyperfine structure parameters with the use of the least squares method in the linear approximation. In the course of the fitting, the parameters of individual doublets were refined. The occupancies of false positions, which were present in the probability distribution function, become negligibly small.

For the magnetic measurements we have used a *Quantum Design MPMS-XLSQUID*-magnetometer. The *dc*-magnetization measurements were made at temperatures of 2–300 K. The magnetization curves *M*(*H*) were measured in a magnetic field up to 50 kOe. The Co-ludwigite samples are highly anisotropic therefore, magnetic measurements have to be made in magnetic fields directed along the different crystallographic axes. In our experiments the sample orientation was determined us-

ing the X-ray diffractometer as shown in Fig. 3. They have been positioned using vacuum grease and fixed with glue to prevent from falling. For the sake of comparison with $Co_3O_2BO_3$ and $Fe_3O_2BO_3$, their magnetic properties, which are not available in the literature, like hysteresis cycles of an oriented single crystal, were measured. During the measurements the cube was adjusted to provide the necessary magnetic field direction relative to the sample and the magnetizations in the *a*, *b* and *c* crystallographic directions were obtained.

Before the magnetic measurements, the single crystals were weighed carefully using a DV 215 CD microbalance. Usually needle-shaped crystals of the transition metal ludwigites obtained by the flux method are very thin and their weight is low. In the case of the parent $Co_3O_2BO_3$ the sample mass was up to 1mg, for Fe-substituted ludwigite – 1.2 mg. The $Co_{2.88}Cu_{0.12}O_2BO_3$ sample chosen for the magnetic measurements weighed only 0.26 mg. The studied $Co_{3-x}Mn_xO_2BO_3$ sample weighed 0.36 mg.

AC-susceptibility measurements were performed in a superconducting quantum interference device (*SQUID*) magnetometer with *ac*-option, in the frequency range $10 < f < 937$ Hz, with an exciting field of 4 Oe. Angle dependent magnetization $M(\theta,T)$ on oriented single crystals were measured with a rotating sample holder option in the SQUID magnetometer up to 50 kOe and with a vibrating sample magnetometer up to a bias field of 90 kOe in the temperature interval 2 – 300 K.

3. LUDWIGTES STRUCTURE AND CATIONIC DISTRIBUTION

The crystallographic structure of the ludwigite single crystals $Co_3O_2BO_3$ and $Co_{2,25}Fe_{0,75}O_2BO_3$ was solved in detail by means of single crystal X-ray diffraction, and the results were given in Table 1. For all compounds the space group is *Pbam*. There are four distinct crystallographic sites for the metal ion in the ludwigite structure. We have numbered these sites as shown in Table 2, which lists the corresponding Wyckoff notation [53]. Metal sites usually also labeled M1 – M4, five O sites labeled O1 – O5, and one B site. The ludwigite crystallographic structure with the numbers of the distinct crystallographic sites are illustrated in Fig. 4. Every cation lies at the center of a distorted oxygen octahedron; the type and degree of distortion are different for each nonequivalent site. Metal sites can be combined as two types of triads. The type I triads are formed by the ions in the positions 4-2-4; the type II triads consist from the ions in the positions 3-1-3. The ensemble of triads determines the low-dimension subunits in the form of three leg ladders (*3LL*). The zigzag walls formed by *3LL* substructures spread along the crystallographic *c* direction.

Table 1. The crystal structure parameters for ludwigite samples

	Co_3BO_5 [32]	$Co_{2,25}Fe_{0,75}BO_5$	Fe_3BO_5 [54]	$Co_{1,7}Mn_{1,3}BO_5$	$Co_{2,88}Cu_{0,12}BO_5$
Molar weight, g/mol	267.6	265.2	264.4	262.48	268.1
Symmetry group	*Pbam*				
Unit cell parameters					
a, Å	9.280	9.282	9.453	9.261	9.299
b, Å	11.928	12.231	12.296	12.328	11.963
c, Å	2.966	3.029	3.072	3.034	2.989
Volume, $Å^3$	328.31	343.92	357.07	346.38	332.48
Density (calc.), g/cm^3	5.414	4.899	-	4.146	4.577

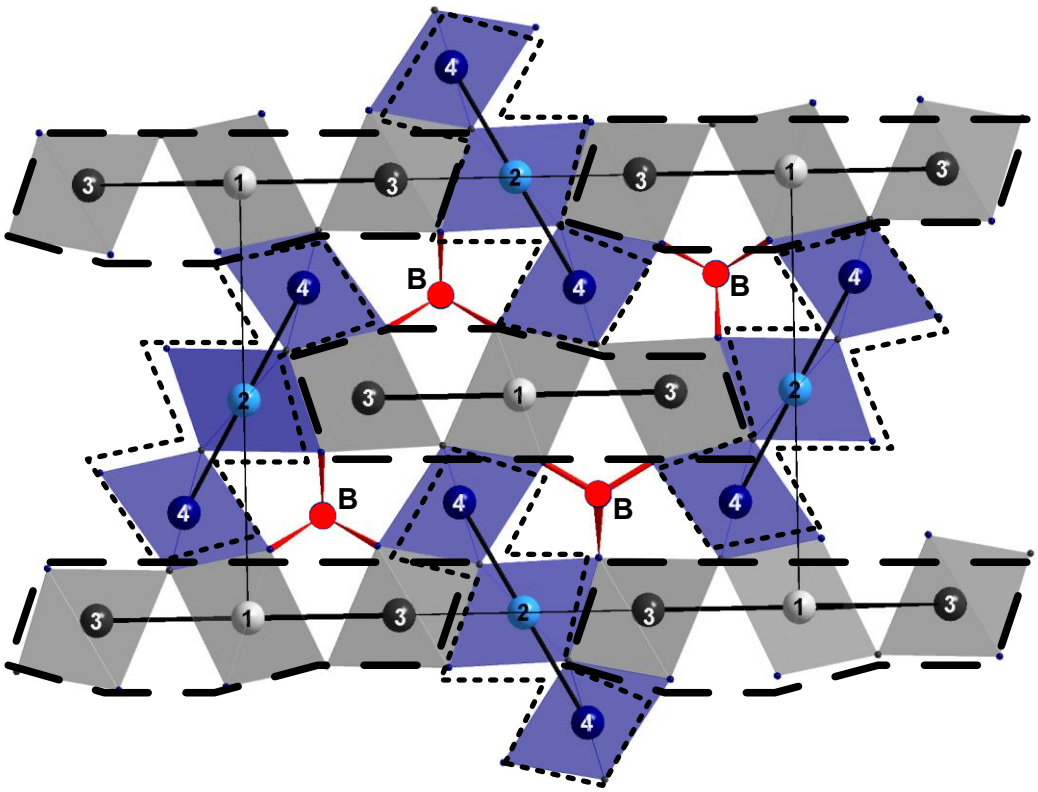

Fig. 4.The cross-section of ludwigite structure perpendicular to *c*-axis. Zigzag walls in the crystal structure of ludwigite is clearly shown. Numbers denote nonequivalent metal sites. Planar BO_3-groups is indicated by three-beam star.Triads 4-2-4 shown by dotted line,3-1-3 – by dashed..

The unit cell parameters for the parent unsubstituted compound $Co_3O_2BO_3$are a = 9.280, b = 11.928, c = 2.966 Å, and unit cell volume is V = 328.31 Å^3. The lattice parameters of the parent compound $Co_3O_2BO_3$ are in a good agreement with those published earlier [55]. Cation distribution and selected bond lengths for the structure at room temperature are listed in the Tables 2 and 3. The atomic coordinates are shown in Appendix. The smallest distance between the metal ions in the present case corresponds to the metal ions at positions 2 and 4 and is less than 3 Å. This is a common feature of the ludwigites with transition metal.The shortest distance in substituted samples is inside the triad 4-2-4 as in the parent $Co_3O_2BO_3$, but it is a little bit larger in the former compound.

Table 2. Cation distribution in crystallographic sites according to X-ray data.

	Co_3BO_5	$Co_{2.25}Fe_{0.75}BO_5$	$Co_{1.7}Mn_{1.3}BO_5$	$Co_{2.88}Cu_{0.12}BO_5$
1	0.25(Co)	0.25(Co)	0.17(Co)+0.08(Mn)	0.25(Co)
2	0.25(Co)	0.19(Co)+0.06(Fe)	0.17(Co)+0.08(Mn)	0.25(Co)
3	0.50(Co)	0.50(Co)	0.33(Co)+0.17(Mn)	0.50(Co)
4	0.50(Co)	0.18(Co)+0.32(Fe)	0.18(Co)+0.32(Mn)	0.44(Co)+0.06(Cu)

For the solid solution ludwigite $Co_{2,25}Fe_{0,75}O_2BO_3$ the lattice parameters are a = 9.282, b = 12.231, c = 3.029 Å. According to the X-ray diffraction data, there is a pronounced preference in the occupation of distinct crystallographic positions by iron ions. The occupancy probabilities of Fe at the 2 and 4 sites are determined to be 0.06245 and 0.31591, respectively, leading to the chemical formula $(Co_{0.5})^1(Co_{0.375}Fe_{0.125})^2(Co)^3(Co_{0.368}Fe_{0.632})^4O_2BO_3$, where the sum of the probabilities at each site is constrained equal to unity. It is seen that iron ions preferably occupy the position 4 that is consistent with the same for $Co_2FeO_2BO_3$ [6], but there is also a small amount of iron ions in the position 2.

Table 3. Metal-metal distances in ludwigite structure. The longest and shortest distances in triads 3-1-3 and 4-2-4 respectively shown by bold.

d, Å	Co_3BO_5	$Co_{2.25}Fe_{0.75}BO_5$	$Co_{1.7}Mn_{1.3}BO_5$	$Co_{2.88}Cu_{0.12}BO_5$	Triad
1-1	2.9660	3.0293	3.0341	2.9890	3-1-3
1-3	**3.2979**	**3.4177**	**3.4380**	**3.3115**	**3-1-3**
3-3	2.9660	3.0293	3.0341	2.9890	3-1-3
2-2	2.9660	3.0293	3.0341	2.9890	4-2-4
2-4	**2.7473**	**2.8141**	**2.800**	**2.7631**	**4-2-4**
4-4	2.9660	3.0293	3.0341	2.9890	4-2-4
1-4	3.0045	3.0280	3.0447	3.0134	
2-3	3.0512	3.0930	3.1197	3.0601	
3-4	3.0847	3.1355	3.1424	3.0947	

The main crystal parameters for the mixed $Co_{1.7}Mn_{1.3}O_2BO_3$ are: a = 9.2800(9), b =11.9278(11), c = 2.9660(3) Å, unit cell volume V= 328.31(6)Å^3. The unit cell volume for the substituted compound $Co_{1.7}Mn_{1.3}O_2BO_3$ exceeds the same for the parent $Co_3O_2BO_3$. The difference is about 5%.It is not surprising because the

ionic radius of a Mn ion is larger than the same for Co ion both in di- and trivalent states(the ionic radii values for high spin ions: Co^{2+} – 0.65, Mn^{2+} – 0.75, Co^{3+} – 0.61 and Mn^{3+} – 0.64 Å) [55]. The thermal parameters U_{eq} have physically reasonable values (See Appendix). The large values U_{eq} correspond to the oxygen ions as for the $Co_3O_2BO_3$ [56].

As it can be seen from the above data the position 4 is the most preferable for the Mn ions similarly to the case of Fe substitution [29]. This position is occupied by about 65% of Mn ions. Nevertheless, this preference is not so brightly pronounced in $Co_{3-x}Mn_xO_2BO_3$ as in $Co_{3-x}Fe_xO_2BO_3$, where the SOFs for the positions 1 and 3 are very small (See Appendix). There is a very significant amount of Mn not only in the position 4, but also in the other three positions, contrary to Fe-substituted compound. These last positions according to our X-ray data, are filled by Mn without any preference, and there is about 30% Mn ions in the each of them.

As it was mentioned above, the SOFs values for the distinct positions allow to define Co : Mn ratio in the compound, which appeared to be near 1.33. Taking into account the distribution of two type of ions among the four nonequivalent sites the chemical formula of compound $Co_{1.7}Mn_{1.3}O_2BO_3$ can approximately be rewritten as $(Co_{0.35}Mn_{0.15})^1$ $(Co_{0.35}Mn_{0.15})^2$ $(Co_{0.67}Mn_{0.33})^3$ $(Co_{0.35}Mn_{0.65})^4O_2BO_3$. It is known that both in $Fe_3O_2BO_3$ and $Co_3O_2BO_3$ the transition ions in the positions 1 and 3 are divalent [34,54]. The triad formed by the ions 4-2-4 consists of three trivalent ions with one extra electron per triad and may be formally considered as two trivalent ions in the positions 4 and one divalent ion in the position 2. Applying this consideration to $Co_{1.7}Mn_{1.3}O_2BO_3$ and proposing that Mn^{2+} substitutes Co^{2+} and Mn^{3+}substitutes Co^{3+}, one can expect almost equal amount of di- and trivalent manganese ions in the investigated compound. Therefore, the average oxidation number Z for Mn ions must be near +2.5. Below, this proposal is checked by the bond valence sum method and magnetic measurements.

As for Cu-substituted sample, the unit cell volume has a value th to parent compound (332.48 $Å^3$) due to the small amount of substituted cation. The chemical

formula of compound Co-Cu ludwigite can approximately be rewritten as $(Co)^1(Co)^2(Co)^3(Co_{0.38}Cu_{0.12})^4O_2BO_3$. Copper ions occupy only the sites numbered 4 where SOF is 0.12. It can be denoted that the affinity of Cu ions with the ludwigite lattice is weak. It could be explained in terms of symmetry: the site 4 in ludwigite structure is more symmetric, while Cu^{2+} ion has d^9 configuration which introduces distortions in the ludwigite lattice.

It seems necessary to mention here that we did not succeed in growing the oxyborates $Co_{3-x}Fe_xO_2BO_3$ with ludwigite structure at $x > 1$. All the attempts have led to obtaining of the crystals $Co_{2-x}Fe_xBO_4$ with warwickite structure [57]. As for $Co_{3-x}Fe_xO_2BO_3$ the crystal growing problems begins near the point where iron totally fills the position 4, specific for trivalent ions. Therefore, probably, the compounds $Co^{2+}_{2-x}Fe^{2+}_xFe^{3+}O_2BO_3$ are unstable and the ludwigite $Co^{2+}_2Fe^{3+}O_2BO_3$ lies at the border of two phases: ludwigite and warwickite. Contrary, in $Co_{3-x}Mn_xO_2BO_3$ the manganese easily enters the ludwigite structure both in divalent and trivalent states.

In order to estimate the valence state of the manganese ions in $Co_{1.7}Mn_{1.3}O_2BO_3$ we have calculated the bond valence sum and obtained the oxidation numbers $Z = \sum_i s_{ij}$ for each of the distinct positions. Here s_{ij}– the bond valence between i and j ions: $s_{ij} = \exp[(R_0 - r_{ij})/b]$, R_0 – the parameter dependent on the nature of ions forming the ij-pair, b – the constant value 0.37 Å, r_{ij} – ij-pair bond length [5, 13-14]. The magnitude of the parameter R_0 for the present ions are taking from [22-24]: R_0 (Co^{2+}) = 1,685 Å, R_0(Co^{3+}) = 1,70 Å, R_0(Fe^{2+}) = 1,734 Å, R_0(Fe^{3+}) = 1,759 Å, R_0(Mn^{2+}) = 1,765 Å, R_0(Mn^{3+}) = 1,732 Å, R_0(Cu^{2+}) = 1,679 Å, R_0(Cu^{3+}) = 1,735 Å, R_0(B^{3+}) = 1,371 Å

Table 4. Cation average valence state in nonequivalent positions.

Position	Co_3BO_5	$Co_{2.25}Fe_{0.75}BO_5$	$Co_{1.7}Mn_{1.3}BO_5$	$Co_{2.88}Cu_{0.12}BO_5$
1	2.00	2.00	2.00	2.00
2	2.00	2.24	2.00	2.24
3	2.00	2.00	2.00	2.00
4	3.00	2.88	3.00	2.88

The Boron atom valence state is typical for all compounds and equal to 2.99. As for metal ions, the average bond valence sum for Mn appeared to be 2.65+, slightly higher than the expected value 2.5+. Thus, both di- and trivalent Mn ions are present in approximately equal amount in $Co_{1.7}Mn_{1.3}O_2BO_3$, contrary to the case of $Co_{3-x}Fe_xO_2BO_3$, where only trivalent Fe ions appeared to enter into the ludwigite structure. Valence state of copper ions are unambiguously determined by this method with the magnitude 2+, that differs from the typical valence in site 4. Table 4 shows the average valence state of each nonequivalent site in the sample with dilution of 3d-metals.

4. MÖSSBAUER SPECTROSCOPY

To prove diffraction data for iron content samples and to determine the valence state of iron ions, the Mössbauer effect study has been done, the results are presented below. As previously described for the ludwigite structure, the shortest pair between the Co(Fe)2 and Co(Fe4) sites with a distance 2.8141 Å. Assuming the competing Co – Fe occupation of only two positions 2 and 4, the relation of atom amounts Co : Fe = 2.96 ≈ 3, which very well corresponds to the proposed chemical formula $Co_{2.25}Fe_{0.75}O_2BO_3$. The crystal structure of $Co_{2.25}Fe_{0.75}O_2BO_3$ projected on the orthorhombic *ab* plane, perpendicular to the *c* axis, is shown in Fig.4. The polyhedra centered at Co and Fe ions are shown. The light polyhedra contain the metal sites Co and Fe, the dark ones contain the Co metal sites.

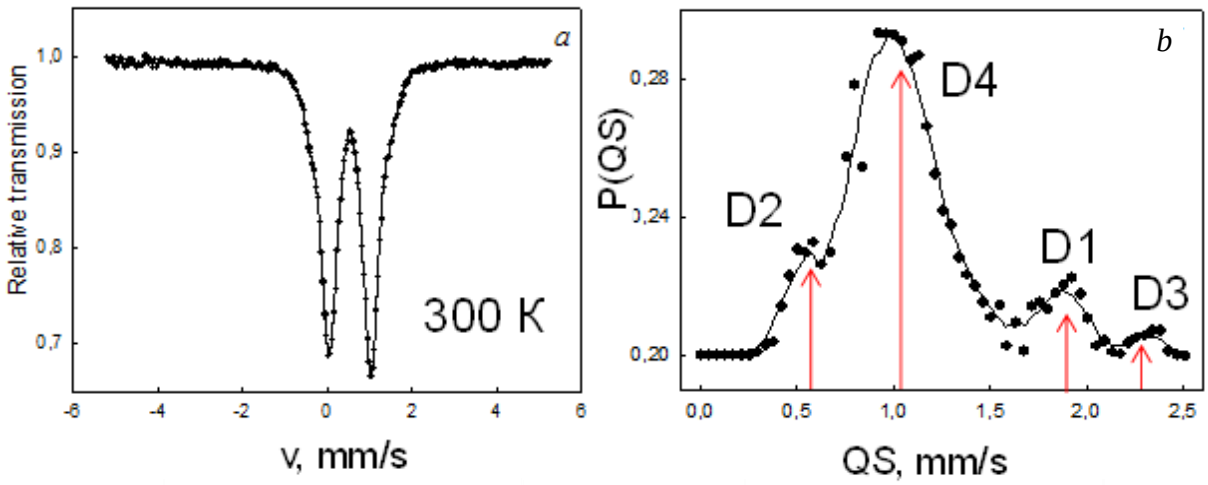

Fig. 5. The Mössbauer spectra of $Co_{2,25}Fe_{0,75}O_2BO_3$ (a) and quadruple splitting distribution *P*(*QS*) calculated from experimental spectra (b). The solid line in the part b fits the experimental results

The Mössbauer spectrum at room temperature presents a sum of quadruple doublets associated with the iron ions occupying nonequivalent crystallographic positions (Fig. 5a). The quadruple splitting *P*(*QS*) distribution was calculated and revealed four maxima that correspond to the four nonequivalent crystallographic posi-

tions (Fig. 5b). The maxima positions were used to form the model spectra. Then the complete row of hyperfine parameters was varied to fit the model to the experimental spectra in the frame of least-squares method in the linear approximation. The results are shown in Table 5.

Table 5. Hyperfine parameters for $Co_{2.25}Fe_{0.75}O_2BO_3$ measured at room temperature. *IS* – the isomer shift relative to αFe (± 0.01 mm/c); *QS* – quadruple splitting at the iron sites (± 0.02 mm/c); *W* – linewidth at half-height for all the Lorentzian used ibn the fitting (± 0.02 mm/c), *SMessb* – iron occupation factor (± 0.03).

IS	QS	W	SMessb	Position
0.38	1.84	0.37	0.10	1
0.39	0.72	0.29	0.18	2
–	~2.2	–	<0.01	3
0.37	1.06	0.38	0.72	4

The isomer shift points out that the Fe ions are trivalent and occupy the octahedral positions 1, 2 and 4. The position 1 is being least occupied, the position 4 is being most occupied and the position 3 is almost free from iron.

To understand why the iron ions clearly prefer the positions 2 and 4, we have calculated the gradient of electric field, created by the oxygen octahedron for every transition metal position in $Co_{2.25}Fe_{0.75}O_2BO_3$ ludwigite. Electric field gradient tensor characterizes the degree of the oxygen octahedral distortion. In the common case, this tensor is nonsymmetrical. Nevertheless, for the qualitative analysis it is sufficient to define only the main tensor component:

$$V_{zz} = 2e\sum \frac{3\cos^2\alpha - 1}{r^3},$$

where α is the angle between the main electric field tensor direction and oxygen anion radius-vector, *r* – the bond *M – O* length, *e* – elementary charge. A point charge model and X-ray data were used. The values of V_{zz} for the four nonequivalent crystallographic positions for all ludwigite series are presented in Table 6, which shows that the oxygen octahedra around the sites 2 and 4 are less distorted in comparison with the octahedra around the site 1 and especially 3. The comparison of the site oc-

cupation data for Mn^{2+} and Mn^{3+} ions with the EFG values for each sites did not reveal any direct correlation between them, as it was in the case of $Co_{3-x}Fe_xO_2BO_3$ [10].

In another words, the field rounding the transition ion, is more symmetric in these two cases. Knowing that Fe^{3+} is d^5 ion, being in *S*-state with a spherically symmetric electron cloud, one can assume that it is the reason for it to occupy the most symmetric states 2 and 4.

Table 6. Calculated EFG value in nonequivalent sites for all studied samples

Position	Co_3BO_5	$Co_{2.25}Fe_{0.75}BO_5$	$Co_{1.7}Mn_{1.3}BO_5$	$Co_{2.88}Cu_{0.12}BO_5$
1	0.171	0.193	0.267	0.160
2	0.204	0.045	0.184	0.018
3	0.281	0.242	0.216	0.234
4	-0.028	-0.017	-0.021	-0.052

In the present work, we aimed to investigate the temperature evolution of the MS spectra in the temperature interval 80–300 K. The spectra were obtained for a powder sample of crushed $Co_{2,25}Fe_{0,75}O_2BO_3$ single crystals (see Fig. 6). At first glance, the most evident feature is the pronounced temperature evolution upon cooling which begins near 110 K, where the splitting of quadrupole doublets into sextets by hyperfine field becomes observable. It is noteworthy to remark that magnetic ordering begins near the same temperature as for $Fe_3O_2BO_3$, while $Co_3O_2BO_3$, much closer in cobalt content to our $Co_{2,25}Fe_{0,75}O_2BO_3$, does not show such a transition.

The second feature that attracts attention is the broadness of MS spectra lines which is much larger than for the parent compound $Fe_3O_2BO_3$ [26], pointing out a high degree of disorder in our system. As we know from our RT X-ray and MS data none of the four distinct crystallographic positions in $Co_{2,25}Fe_{0,75}O_2BO_3$ is totally filled by iron or totally free from it. Therefore, even being in the same crystallographic position, iron ions can have different number of Co and Fe ions among their neighbors, different degree of oxygen octahedral distortion, and possible different

oxidation state. All these factors prevent the true assignment of MS spectra lines from the fitting.

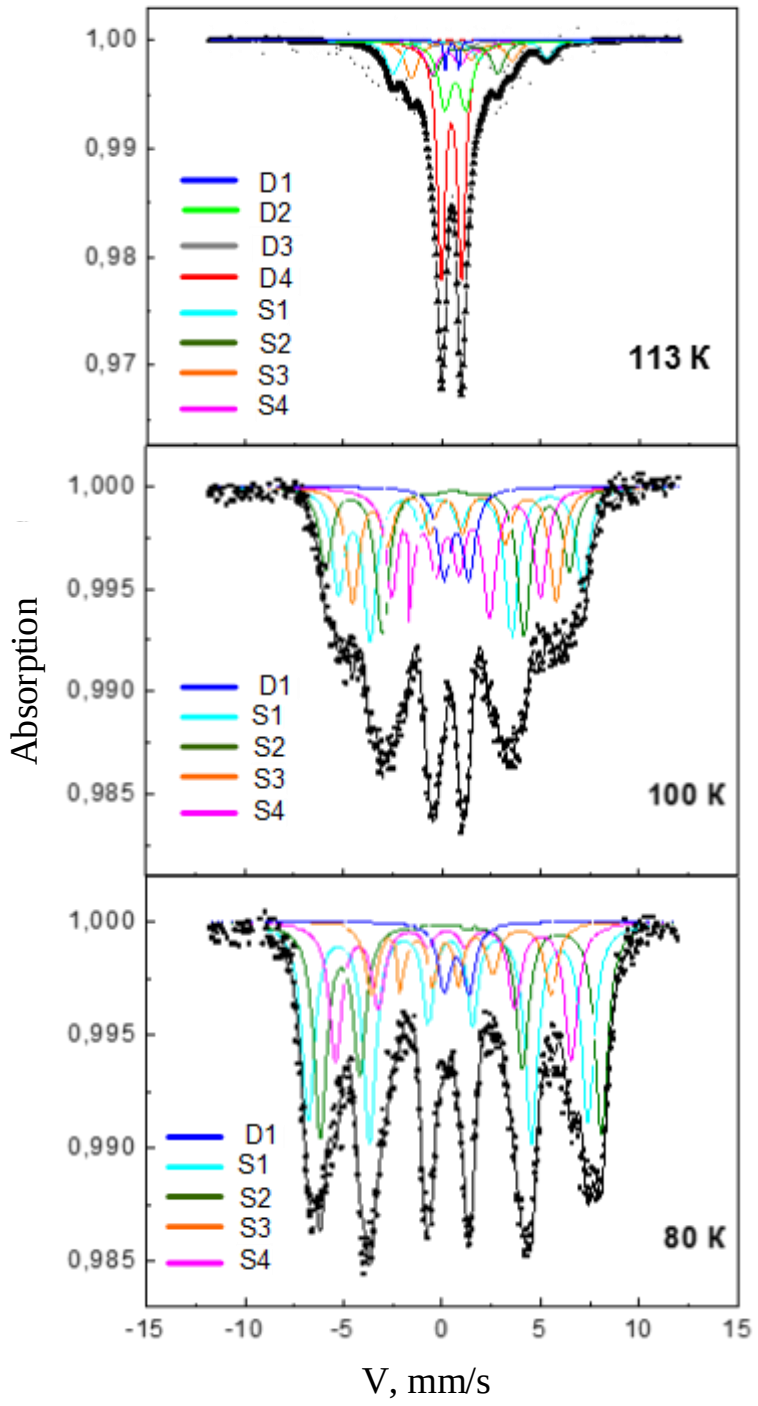

Fig. 6. Mössbauer spectra of $Co_{2,25}Fe_{0,75}O_2BO_3$ at different temperatures.

Nevertheless, at high temperatures down to T =120 K the MS spectra can be well described by four doublets. The isomer shift values δ for three of them (D2, D3 and D4, Fig. 6) are typical for iron ions in the trivalent state. For the doublet D1 the isomer shift value is higher and indicates that there are iron ions with a valence state less than 3. The temperature dependence of the isomer shift values in the paramagnetic state shown in Fig. 7 are close to those for $Fe_3O_2BO_3$ [26]. However, contrary to [26] now there is no contribution from the ions with $\delta > 1$ mm/s (typical for Fe^{2+}). One of the doublets marked in Fig. 7 as D4 clearly dominates in the area, so it seems possible that it corresponds to the trivalent iron in the position 4. Between 110 and 120 K the splitting of the doublets begins and below 110 K the MS spectra may be described by four sextets and one low area doublet with $\delta = 0.75$ mm/s and quadrupole splitting $Q = 1.25$ mm/s. In the paramagnetic state, this doublet is depicted by D1 line in Fig. 7. Note that the authors of [26,34] also have described the MS spectra for the parent $Fe_3O_2BO_3$ between 70 and 115 K by some sextets and one doublet. They have assigned it to the divalent iron ions in the position 1. According to MS data [34], only these ions are magnetically disordered in $Fe_3O_2BO_3$ down to $T = 70$ K, at the same time the other Fe ions order magnetically near $T = 110$ K. In our case this doublet also probably corresponds to the iron ions in the position 1, but its relative contribution is small (about 5 per cent in area). Moreover, the isomer shift value for this doublet is closer to $Fe^{2.5+}$ and not to Fe^{2+}.

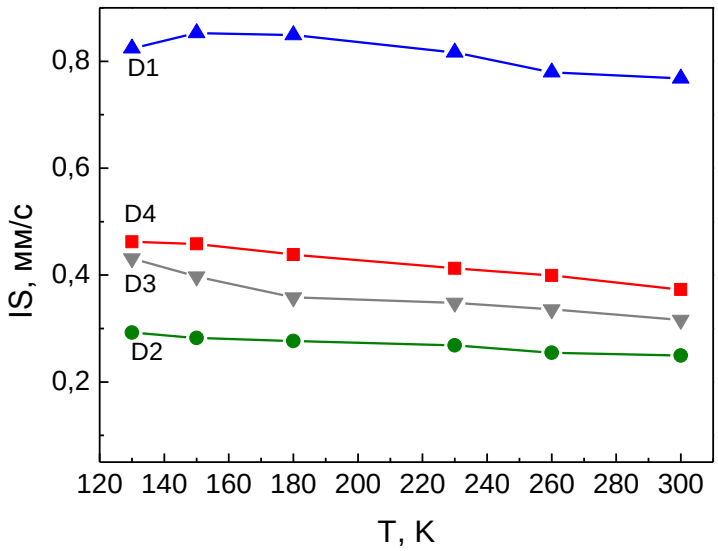

Fig. 7. Paramagnetic state: the isomer shift temperature dependencies.

Below T = 110 K the isomer shift and quadrupole splitting values for the iron in the dominant position 4 are temperature independent (δ = 0.46 mm/s, Q = 1.0 mm/s) and the hyperfine field B_{hf} increases as the temperature decreases (Fig. 8).

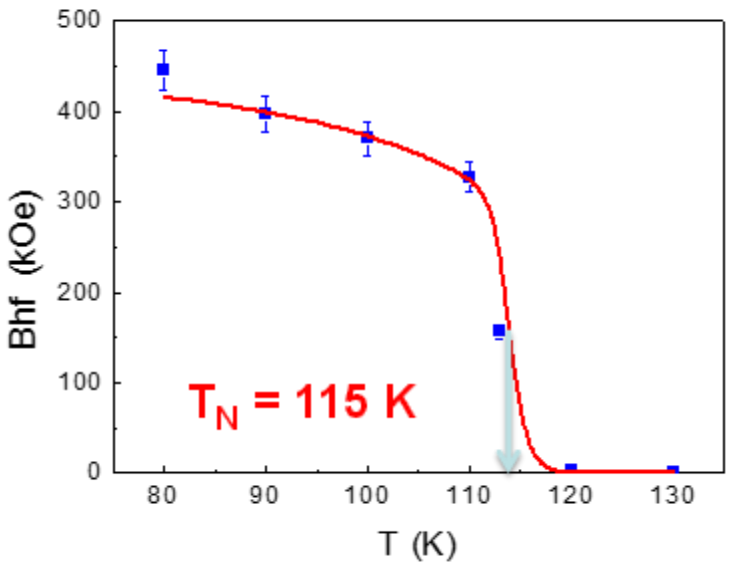

Fig. 8. The hyperfine field temperature dependence for the iron ions in the position 4.

Comparing our MS data for $Co_{2,25}Fe_{0,75}O_2BO_3$with the same obtained for the parent compound $Fe_3O_2BO_3$ one can conclude that the picture is very similar in both cases, but in the solid solution compound the MS spectra lines are broader because of high degree of disorder. For this reason it is hardly possible to define the contribution of each iron state to our MS spectra. However, we clearly see the onset of magnetic ordering near 110 K as in $Fe_3O_2BO_3$. Thus, a fraction of the magnetic ions remain disordered down to 70 K. Probably they are iron ions in crystallographic position 1, but in our case of $Co_{2,25}Fe_{0,75}O_2BO_3$ their contribution is small.

5. MAGNETIC PROPERTIES OF LUDWIGITES

In this section the results obtained from rotating angle *M(θ,T)* and *M(H)* measurements for the parent compounds $Co_3O_2BO_3$ and $Fe_3O_2BO_3$ are presented. This facilitates the understanding of the $Co_{2,25}Fe_{0,75}O_2BO_3$ magnetic properties. It is known that in both Co and Fe pure compounds the *c* axis is a hard magnetization direction, therefore only the anisotropy in the *ab* plane has been studied below. Results of magnetic properties for Mn- and Cu-substituted samples are presented below the accurate study of Co-Fe ludwigites.

5.1 Magnetic behavior of $Co_3O_2BO_3$

This compound has just one magnetic phase transition to a ferromagnetic phase at T_C=42 K [53]. In *M(θ,T)* measurements we could determine that the easy magnetization direction (EMD) in the ordered phase is the *b* axis (not shown). In Fig. 9 the hysteresis cycles for the compound $Co_3O_2BO_3$, measured below T_C on a single crystal along its *b* axis, are given. Though the remanence magnetization M_r =3.4(1) μ_B/f.u. remains practically constant, the coercive field H_c increases as temperature is lowered. The small slope of *M(H)* at high fields indicates the existence of a small superimposed antiferromagnetic susceptibility, with the value χ_{AF}=0.024(1) (emu/mol) (see Table 7). Besides, in the hysteresis cycles measured at fixed temperature *T*=2 K, Fig. 10, the coercive field increases when the angle θ_H between the applied field and the *b* axis increases, following a 1/cos θ_H dependence.

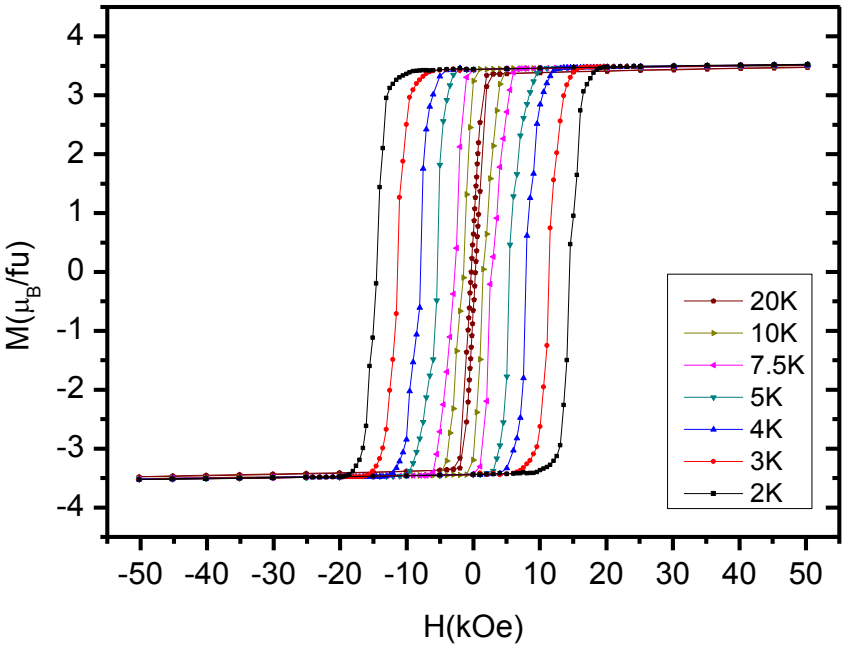

Fig. 9. Hysteresis cycles $Co_3O_2BO_3$ sample as a function of T ($T < T_N$). H parallel to b axis.

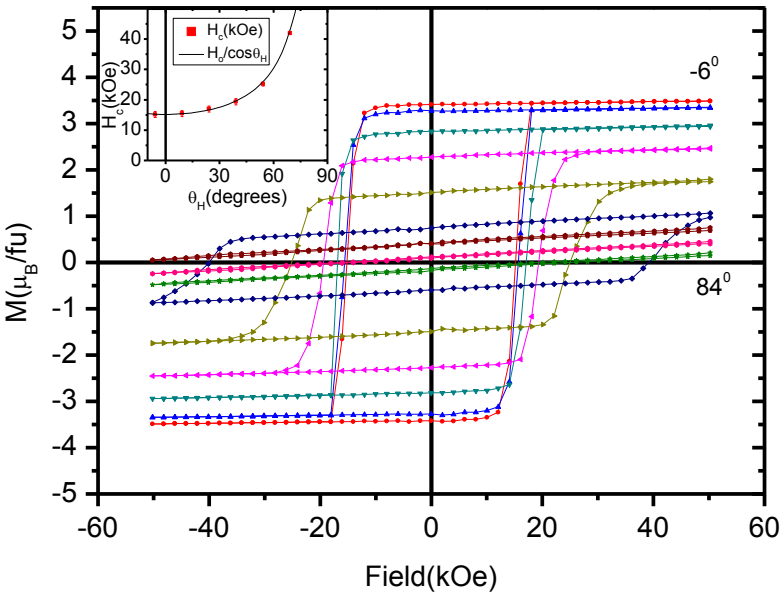

Fig. 10. Hysteresis cycles of a $Co_3O_2BO_3$ single crystal at T=2 K, as a function of rotation around the c axis. The extreme values of θ_H are indicated. The inset shows the variation of $H_C$as a function of θ_H. The fit to a $1/cos\theta_H$ function is also shown.

5.2 Angular magnetization dependencies of $Fe_3O_2BO_3$

This compound is known to undergo a charge order transition at T_{CO}=283 K, and 3 successive magnetic transitions as temperature is lowered (P-AFM1-F-AFM2). The transition temperatures we have measured are T_{N1}=110.7 K, T_{N2}=69.2 K, and T_{N3}=30. K, in reasonable agreement with previous findings [34]. It is convenient to remember in the discussion below that in all ordered phases the Fe_2 and Fe_4 sublattice magnetizations are parallel to the *b* axis. Nevertheless, only in the F phase the Fe_1 and Fe_3 sublattice magnetizations bear a non-zero moment along the *a* axis, as determined from NPD measurements [28], and the AFM2 phase could not be discerned from NPD. However, MS gave evidence of this low temperature phase when the θ angle between B_{hf} and V_{zz}(electric field gradient) for the different Fe sites became different from those in the AFM1 or F phases [34].

Surprisingly the detailed magnetization anisotropy directions of the different phases in this much studied compound have not been unambiguously determined up to date since the measurements were performed on randomly oriented powder or small collections of crystals. To unravel this question the same methodology of rotating sample magnetometry around the *c* axis has been applied to a $Fe_3O_2BO_3$ single crystal. In Fig.11, where the $M(\theta,T)$ data measured at 50 kOe are shown, it is evidenced that the antiferromagnetic phase AFM1($T_{N1} > T > T_{N2}$) is anisotropic, with the *a* axis as EMD at H=50 kOe. Below T_{N2}, the ferromagnetic phase F is strongly anisotropic, with *a* axis as EMD. The magnetization reversal process is characteristic for a system of anisotropy field much higher than the coercive field (see below).

In Fig. 12 the hysteresis cycles measured along the *a* direction at different temperatures are depicted. As the compound is cooled from room temperature, at T_{N2} the F phase cycle opens, as expected for a ferrimagnetic phase. The coercive field increases with decreasing temperature and the remanence M_r decreases. At T=30 K there is no coercivity and M_r becomes zero, as the system transforms into the new AFM2 phase (see Fig. 12 inset). This temperature is 9 K lower than T_{N2} reported earlier [28]. In stark discrepancy with the value of M_r=2.65 μ_B/f.u. deduced

from the NPD, we find that $M_r(T_{N2})$≈0.16 μ_B/f.u., which, on the other hand, is in good agreement with the value given in Ref. 4 for a collection of crystals (≈0.1 μ_B/f.u.). Additionally, in NPD it was found that the Fe_3 and Fe_1 magnetic sublattices give rise to the ferrimagnetic character since they have opposite contributions to the magnetization in the *a* direction [28]. Therefore, the reduction of M_r indicates that there is a compensation process of the Fe_1 and Fe_3 sublattice magnetization as temperature decreases below T_{N2}.

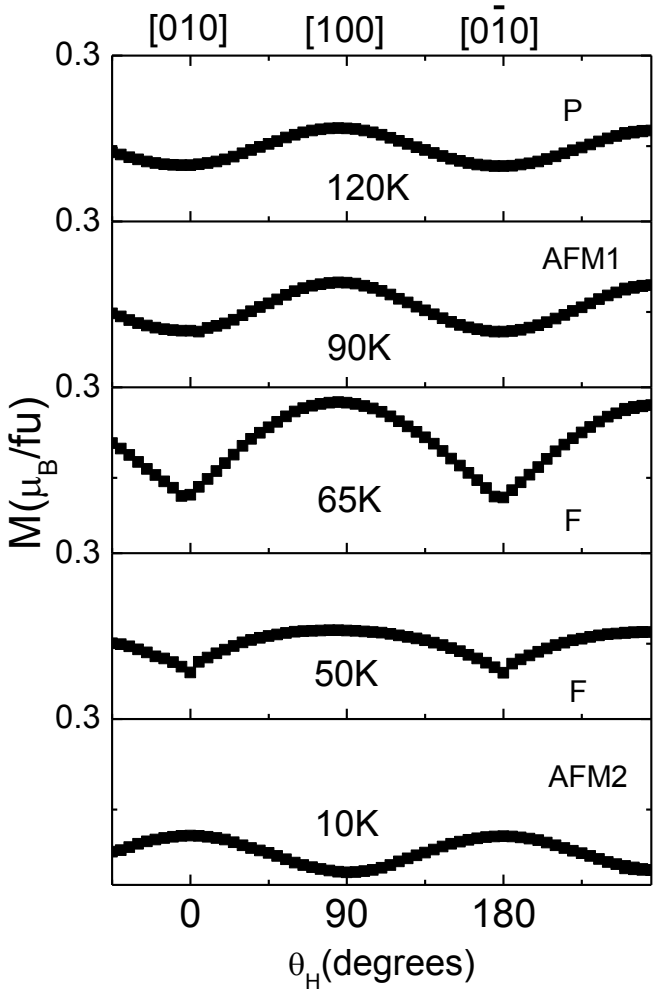

Fig. 11. The projection of the magnetization of $Fe_3O_2BO_3$ in the direction of the applied field upon rotation around the *c* axis. *H* = 50 kOe. Note the change of anisotropy EMD at 10 K <T_{N3} to the *b* axis, while at all other temperatures it is along the *a* axis.

The high-field slope of the hysteresis curves allows us to determine the subjacent antiferromagnetic susceptibility χ_{AF} (T) (see Fig. 12 inset). It has the temperature dependence of an antiferromagnetic system measured along the parallel direction, with ordering temperature at the point of maximum slope below the maximum, which corresponds nicely to the T_{N2} temperature. Since only below this temperature Fe_1 and Fe_3 sublattice moments become nonzero, as observed by NPD, it can be stated that these sublattices are at the origin of the AF subjacent susceptibility along the *a* axis. This interpretation is slightly different from the conclusion reached from MS that only Fe_1 sublattice orders at T_{N2} [34]

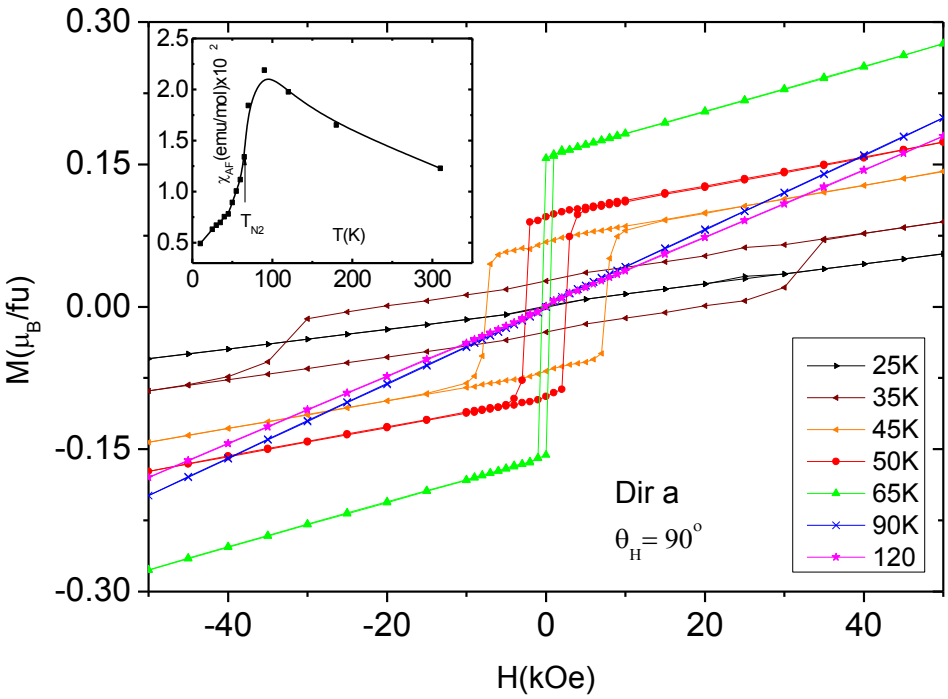

Fig. 12. Selected hysteresis cycles of $Fe_3O_2BO_3$ sample at different temperatures, with *H* parallel to *a* axis. Inset. Subjacent antiferromagnetic susceptibility χ_{AF} in the *a* direction, determined from the high field slope of the *M(H)* cycles.

$M_a(T)$ and $M_b(T)$, measured at 50 kOe along the *a* and *b* axis, respectively, illustrate this compensation behavior clearly (Fig. 13). The transition at T_{N1} gives rise to a change of slope in M_b only, while the transition to the ferromagnetic ordered phase at T_{N2} shows a peak in both $M_a(T)$ and $M_b(T)$, as could be expected for the establishment of ferrimagnetism [40]. Below T_{N2} there is a decrease in $M_a(T)$ as a conse-

quence of the progressive compensation of the Fe_1 and Fe_3 sublattice magnetization. In fact, at $T_{N3}M_a(T) = M_b(T)$ and the anisotropy is planar within the *ab* plane. Below this temperature, *b* is the EMD of the anisotropic AFM2; i.e. orthogonal to that in the AMF1 or F phases.

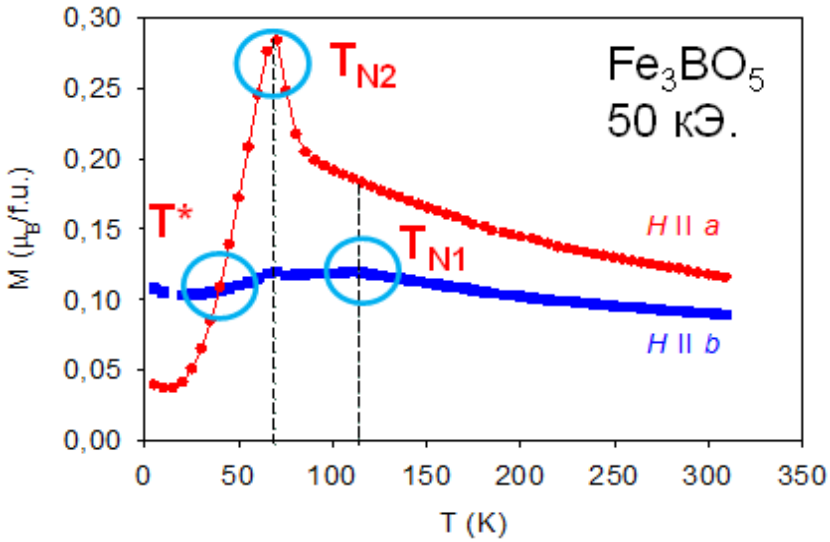

Fig. 13. $M_a(T)$ and $M_b(T)$ measurements for $Fe_3O_2BO_3$

5.3 Magnetic properties of mixed $Co_{2.25}Fe_{0.75}O_2BO_3$ludwigite.

First, the evidence for the presence and character of the magnetic phase transitions in this compound is obtained from the temperature dependent susceptibility and magnetization measurements, and later the anisotropy of the single crystal is analyzed by means of the angle dependent magnetization and hysteresis cycles data.

5.3.1 Magnetization temperature dependence.

Field cooled (FC) and zero field cooled (ZFC) single crystal dc magnetization measurements were performed with an applied field of 100 Oe and 600 Oe on a single crystal. As it is seen in Fig. 14 there is a sharp increase of the FC and ZFC magnetization near T = 70 K (Fig. 14), then FC value decreases when cooling and ZFC drops to zero, being peak-like. Comparing the present data for $Co_{2.25}Fe_{0.75}O_2BO_3$ with the same

obtained in [29] for $Co_2FeO_2BO_3$, one can see that they are very similar. The shape of magnetization temperature dependence is closer to $Fe_3O_2BO_3$ [30], and it is rather different from the same for $Co_3O_2BO_3$ [58]. There is no sign of the magnetic ordering at 42 K; i.e. the characteristic temperature of $Co_3O_2BO_3$, indicating the absence of hetereogenity in the sample.

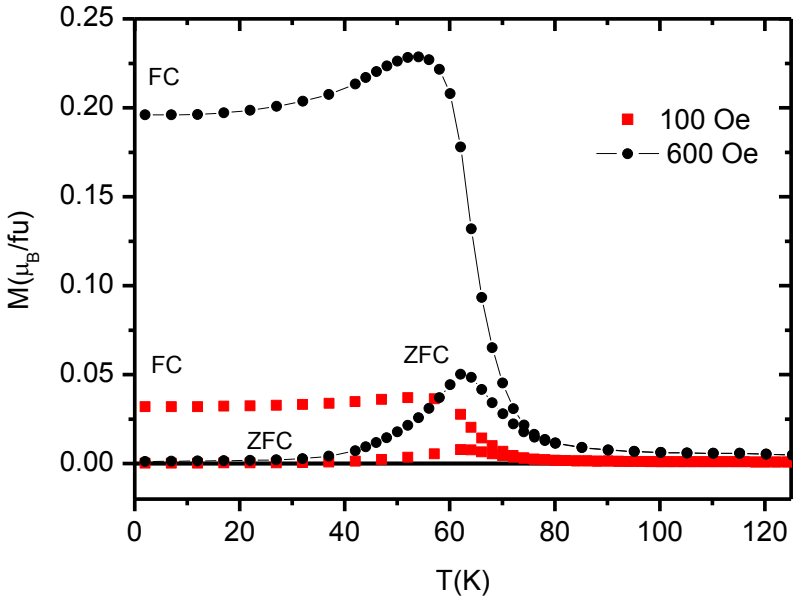

Fig. 14. The magnetization temperature dependence of a $Co_{2,25}Fe_{0,75}O_2BO_3$ single crystal.

5.3.2 AC magnetic susceptibility.

The F transition can be clearly observed in *ac* magnetic susceptibility temperature dependence at T_C = 70 K. For these measurements, a single crystal was not large enough to give a good signal to noise ratio, so the collective signal for several samples was measured. The temperature behavior of real χ' and imaginary χ'' components of magnetic susceptibility is shown in Fig. 15, where a large peak at 70 K and a small anomaly near 115 K are visible. The latter is reminiscent of the AFM1 transition in $Fe_3O_2BO_3$ and corresponds to the beginning of magnetic ordering in our material seen from the temperature dependence of the MS hyperfine field. The large susceptibility peak is frequency dependent, pointing to domain wall motion of the ferrimagnetic

domains. This peak is slightly shifted to higher temperature as the frequency increases.

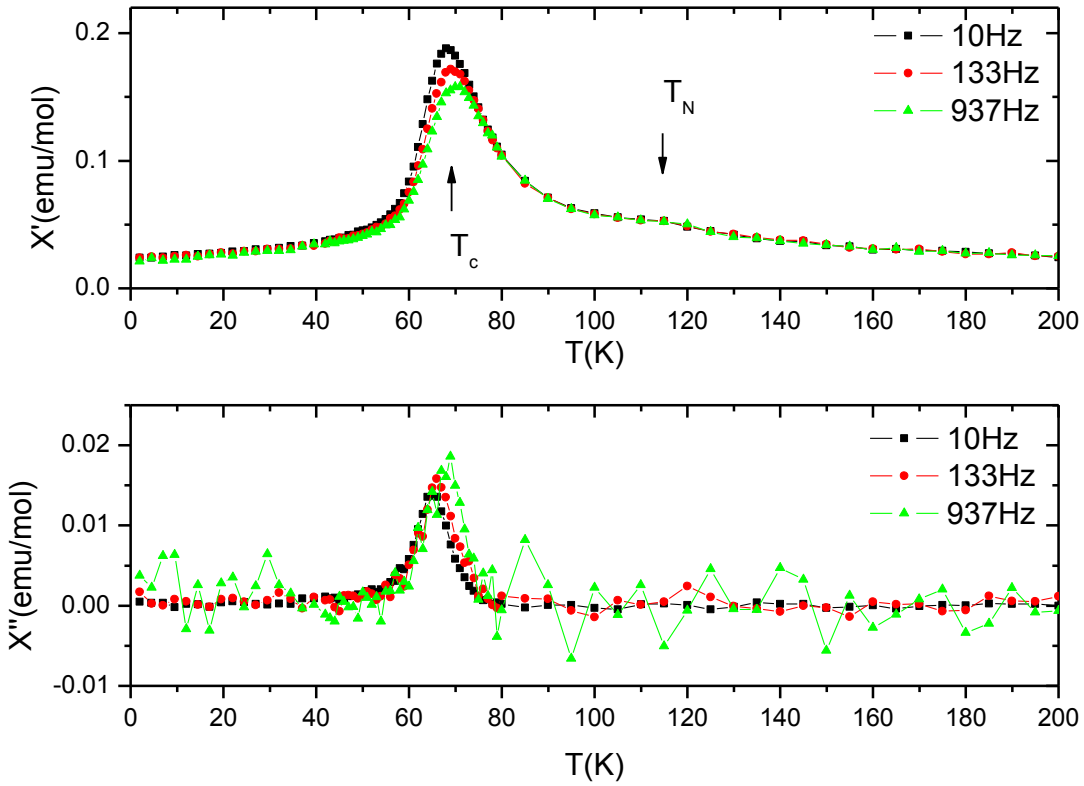

Fig. 15. The real and imaginary components of $Co_{2,25}Fe_{0,75}O_2BO_3$ magnetic susceptibility temperature dependences. The arrows point the magnetic transitions: a large peak near 70 K and a small anomaly near 115 K.

These ac-susceptibility data are also very similar to those for $Co_2FeO_2BO_3$ [29]. The analysis of the χ_{dc}^{-1} obtained with the ZFC measurements allows determining the Curie constant C and the Curie-Weiss temperature θ_C. The results are given in the Table, together with the values for the end members of the row and $Co_2FeO_2BO_3$ [29]. For all compounds, the θ_C value is negative, pointing out the predominance of antiferromagnetic interactions. The module of θ_C increases with Fe content in a regular trend. Consequently, the AF component of exchange interactions value is higher for iron ions than for cobalt ions. Our results are in the whole consistent with those previously obtained except the value of the effective magnetic moment in the paramagnetic

phase, which in $Co_{2,25}Fe_{0,75}O_2BO_3$ is closer to $Co_3O_2BO_3$ than to $Co_2FeO_2BO_3$, as shown below. Earlier, the authors of [13, 14] have defined the effective magnetic moments values averaged for one magnetic ion. In our Table 7 their results are recalculated to effective magnetic moment per formula unit. As for the effective magnetic moment of $Fe_3O_2BO_3$, defined in [30], there are some questions about it. The authors of [4] claimed the effective magnetic moment to be 6.6 μ_B. At the same time their value for Curie constant C = 10.9 $\frac{emu \cdot K}{mol \cdot Oe}$ in our opinion gives μ_{eff} = 9.34 μ_B per formula unit. Namely, this value is presented in the Table 7 (Column 4) for comparison. All the values calculated by us using the data of [29,30,53] marked by an asterisk (*).

5.3.3Magnetic hysteresis.

The main characteristic of $Co_{2.25}Fe_{0.75}O_2BO_3$ is its high anisotropy. Indeed, with the rotating sample holder option which allows to measure the projection of the magnetization along the field direction it was found that the easy axis of magnetization is *b*, [010] axis. This is evidenced in Fig. 16, where $M(\theta,T)$ at H= 50 kOe and different temperatures as a function of the applied field angle θ_H with respect to the *b* axis, when the sample is rotated around the *c* axis, are given.

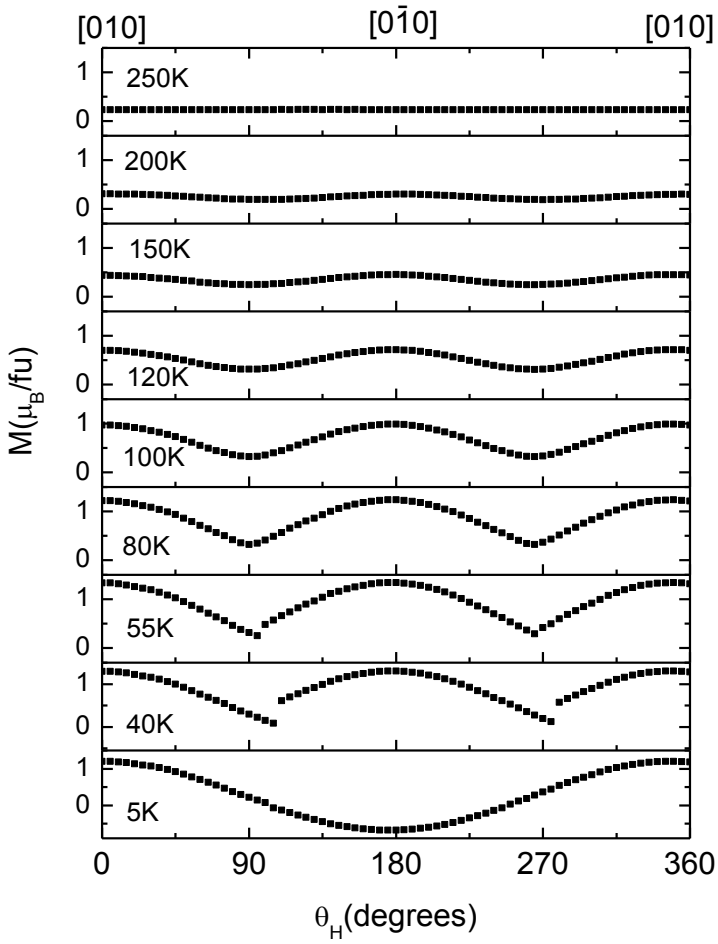

Fig. 16. The projection of the magnetization of $Co_{2,25}Fe_{0,75}O_2BO_3$ in the direction of the applied field upon rotation around the *c* axis. *H* = 50 kOe.

At this field and *T*=5 K the anisotropy along the *b* axis is so strong that the magnetization remains oriented along that axis in a 180° revolution, and *M(θ)* is fitted with a cosine function superimposed to a constant antiferromagnetic component. This proves without any ambiguity that the magnetic anisotropy of this crystal is uniaxial along the *b* axis direction, and implies that at this field and temperature the crystalwas saturated in the single domain state. When temperature rises, the anisotropy decreases, so that above a certain temperature the applied constant field is capable of inducing magnetization reversal from the [010] direction to the $[0\bar{1}0]$ direction (Fig. 17, 40 K). The reversal of the magnetization is very abrupt, that is, the effect due to the field component perpendicular to the *b* axis is reversible but very small, and remains so till

the magnetization reversal, while the magnetization reorientation in the *b* direction is irreversible. Therefore, the field component parallel to the *b* axis produces the magnetization reversal when $H\cos\theta_H \approx H_C^b$, where H_C^b is the coercive field in the *b* direction. This behavior is characteristic for systems where the coercive field is much weaker than the anisotropy field. The magnetization reversal cannot be at unison, but instead by curling or buckling, and appearance and displacement of domain walls within the sample. It is noteworthy that the anisotropy remains visible above T_C and T_N, up to the paramagnetic phase. The coercive fields at 20, 30 and 40 K could be determined by the angular rotation of the applied field method (Fig. 16, for T = 40 K). We have obtained the following $H_c$values, 44 kOe, 22 kOe and 13 kOe at 20K, 30K and 40 K, respectively. As we will see below, these values are similar to the values found from actual hysteresis loops.

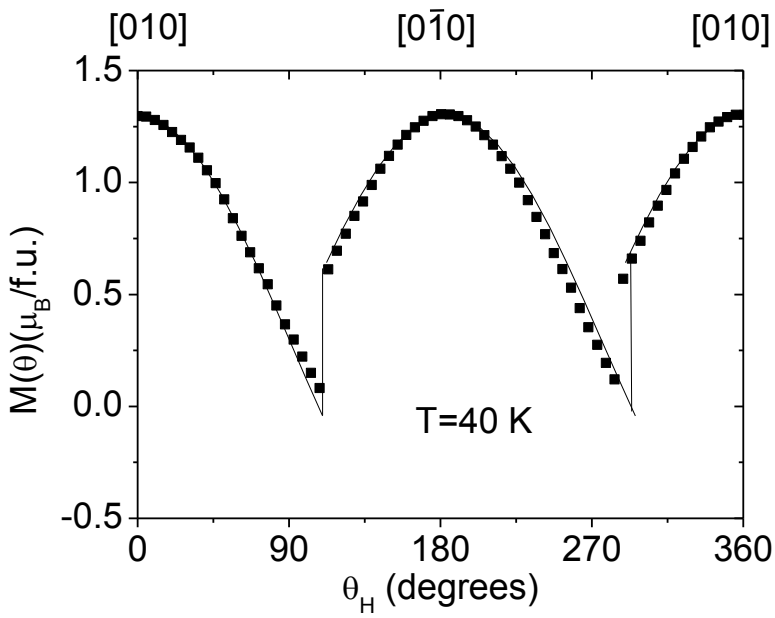

Fig. 17. The projection of the magnetization of $Co_{2,25}Fe_{0,75}O_2BO_3$ in the direction of the applied field upon rotation around the *c* axis. Note the moment reversion at 110° and return at 288°.

The $Co_{2,25}Fe_{0,75}O_2BO_3$ is highly anisotropic, therefore the *M(H)* hysteresis cycles have been measured at several temperatures in the directions parallel to the *c* axis and perpendicular to it (*b* axis) on a single crystal (Fig. 18), in the temperature range 70

<T< 115 K. In the *c* direction the material behaves as a simple antiferromagnet with a linear magnetization curve at all measured temperatures. Thus, the magnetic moments in the compound are fully compensated in the *c* axis. In contrast, in the *b* direction the hysteresis cycles below 115 K shows an increase in the magnetization which indicates that already non compensation of the moments sets on below that temperature. Below T_C the hysteresis cycle is open, thereby showing the existence of ferro- or ferrimagnetic ordering. Both curves tend to the same high field limit, which indicates that the Co sublattice is already contributing to the magnetization in the region $T_C<T<T_N$, but since the Co sublattice is not yet magnetically ordered it is due to polarization of the Co moments by the Fe ordered sublattice.

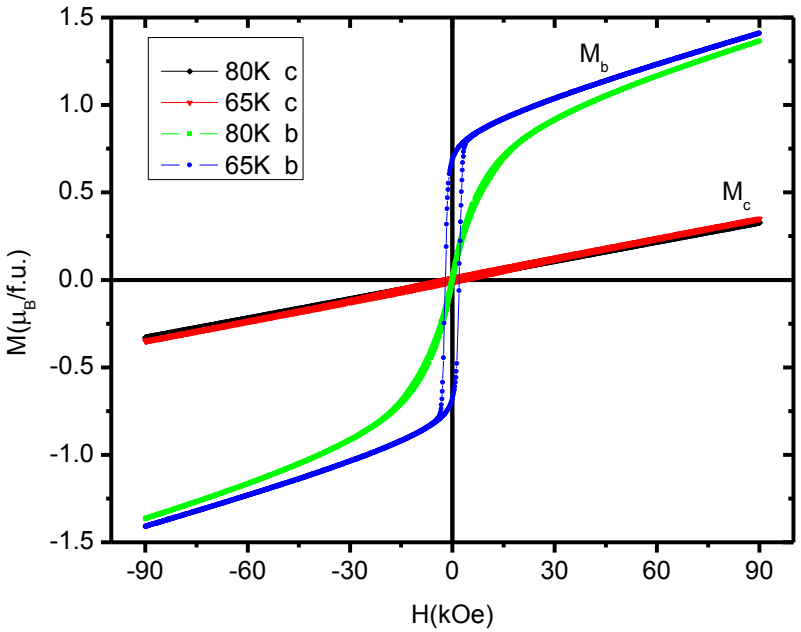

Fig. 18. Hysteresis cycles as a function of T $(T \geq T_N)$.H applied along the *b* and *c* axes.

The coercive field increases drastically as temperature is lowered (Fig.19), with a measured maximum H_C^b=90 kOe at 10 K. Below that temperature the coercive field becomes larger than the maximum applied field, 90 kOe, of our set up. This is an extraordinary high coercivity. Superimposed to this fascinating feature is an AF component, expressed as the absence of saturation and linear dependence of the magnetiza-

tion with the field at high fields. This behavior is characteristic for an uncompensated antiferromagnet, or a ferrimagnet. Thus, the high field branches of $M(H)$ are not saturated, but have a positive slope χ_{AF}. The maximum values of χ_{AF} obtained for our sample and those of $Fe_3O_2BO_3$, $Co_3O_2BO_3$ and $Co_2FeO_2BO_3$ [29,30,53,59] are quite close to each other: $\chi_{AF} \approx 0.03$ emu/mol (see the Table). That is, there are several sublattices with AF coupling but with incomplete compensation in this material. It was found that χ_{AF} is practically isotropic at a fixed temperature. Besides, the remanent magnetization M_r is almost independent of T at low temperatures, and at the coercive field the difference between the magnetization in the up and down orientations is $\Delta M=2M_r$, which implies that the ferromagnetic component of the magnetization is saturated at a value $M=M_r$. The remanent magnetization M_r and *dc* susceptibility values χ_{AF} extracted from hysteresis loops are collected in the Table 7 together with the data obtained earlier in [29,30,53,59] for $Fe_3O_2BO_3$, $Co_3O_2BO_3$ and $Co_2FeO_2BO_3$.

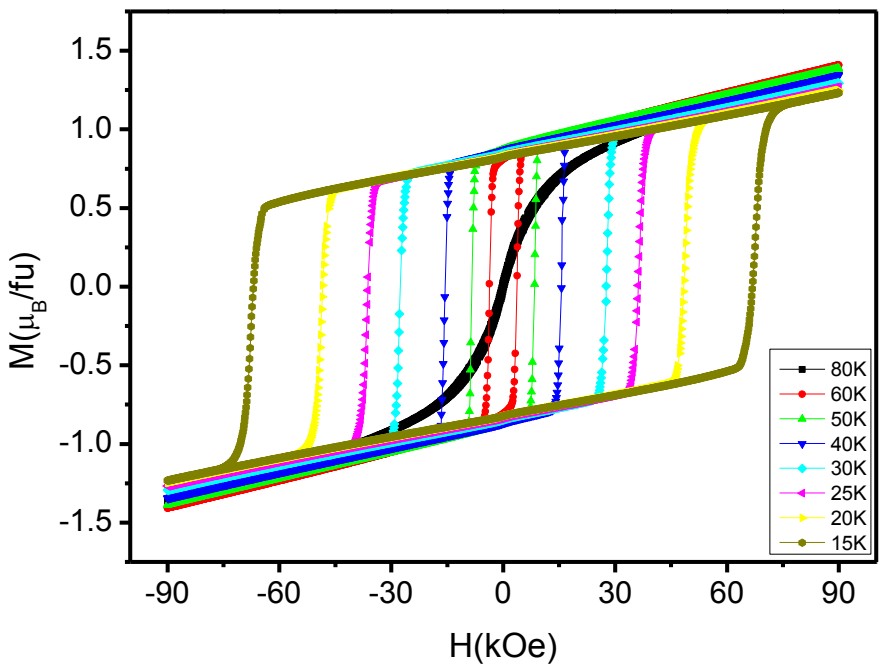

Fig. 19. Hysteresis cycles of $Co_{2,25}Fe_{0,75}O_2BO_3$ sample as a function of T ($T < T_N$).H parallel to b axis.

In Fig. 20 the $H_C(T)$ curves found for the three samples are compared along their corresponding EMD. For $Co_3O_2BO_3$, $H_C(T)$ in the b direction increases only below 10

K, while for $Fe_3O_2BO_3$ H_C^a increases rapidly as temperature decreases once the F phase is reached at T_{N2}, and becomes zero below T_{N3}. It becomes evident that there is a strong increase of $H_C^b(T)$ upon Fe substitution of Co, i.e. at T=10 K the ratio of H_C^b between that $Co_{2,25}Fe_{0,75}O_2BO_3$ and $Co_3O_2BO_3$ is about 40.

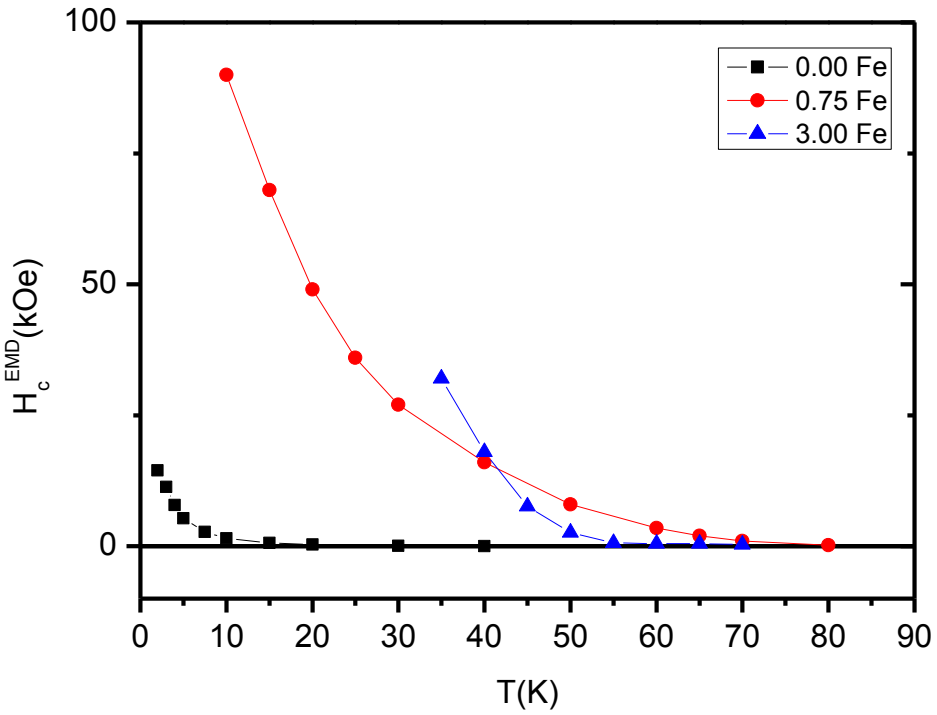

Fig. 20. $H_C^b(T)$ for$H$ parallel to b axis. The data for $Co_{2,25}Fe_{0,75}O_2BO_3$ (●), $Co_3O_2BO_5$ (■) and $Fe_3O_2BO_3$ are shown.

Table 7. Collected magnetic transition temperature data for $Co_{3-x}Fe_xO_2BO_3$ from χ_{ac}, Easy Magnetization Direction at $T<T_C$, high T susceptibility (Columns 5-8) and hysteresis cycles. By (*) we mark the values, calculated by us using the data presented in [29,43,58]. In bold, present work results.

x	0	0.75	1 [29,33]	3
$T_{N3}(K)$		53		50, **30**
$T_C(K)$, $T_{N2}(K)$	42	**70**	70	74
$T_N(K)$, $T_{N1}(K)$		**115**	117	112
EMD ($T<T_C$)	***b***	***b***	?	*a*
μ_{eff}/f.u.(μ_B)	**7.20**	**7.28(2)**	7.53	**8.01, 9.34***
μ_S/f.u.(μ_B)	**7.35**	**7.89**	**8.06**	**9.11**

μ_J/f.u.(μ_B)	**5.52**	**6.27**	**6.51**	**9.01**
θ_C(K)	**-25**	**-69(3)**	-82	**-436**
M_r (μ_B/f.u.)	1.8*, **3.4(1)**	**0.9(1)**	0.48*	2.36*, **0.16**
χ_{AF}(emu/mol)	**0.024(1)**	**0.029(3)**	0.036*	0.020*

As can be seen for $Co_{2,25}Fe_{0,75}O_2BO_3$ (Fig. 21, inset) when the external field is applied at an angle θ_H from the *b* direction the coercive field increases approximately as $1/\cos\theta_H$ (Kondorsky law) [60]. The same dependence is found for $Co_3O_2BO_3$ (Fig. 10, inset). It is justified at low temperatures in view that the $M(\theta_H)$ curves can be fitted with the expression:

$$M(\theta_H) = M_r \cos\theta_H + \chi_{AF} H$$

As mentioned above, the compliance of this $1/\cos\theta_H$ dependence of the angular dependence of the coercive field is characteristic of coercive fields smaller than the anisotropy field. The reason for this behavior may be stress anisotropy or defect pinning of domain walls. Since we are dealing with a single crystal we do not expect stress as an origin of anisotropy but, on the other hand, it is a substitutional system, where many defects in the crystal may be present, therefore, pinned domain walls may account for the coercive field. The coercive field in the *b* direction due to this mechanism, with 180º domain walls being created and propagated at the switching field gives a coercive field:

$$H_C^b(\theta_H) = \frac{\gamma}{\cos\theta_H l M_r},$$

where γ is the domain wall energy and l is the average defect-defect distance. The temperature dependence of this coercive field enters via the dependence of the wall energy on the anisotropy constant K_1, $\gamma \propto \sqrt{AK_1}$, where A is proportional to the exchange coupling [61]. For comparison sake, at the same temperature T=10 K, and θ_H=0 one obtains, $H_C^b M_r = \frac{\gamma}{l}$=8.73 x 10^6 and 7.46 x 10^5 G^2 for $Co_{2,25}Fe_{0,75}O_2BO_3$and $Co_3O_2BO_3$, respectively, i.e. an order of magnitude increase upon the Co substitution by Fe. Since $T_c$is larger and therefore A is larger for $Co_{2,25}Fe_{0,75}O_2BO_3$, but not enough

to explain the observed increase, and K_1 may be similar in both compounds.It can be concluded that the main reason for the increase in coercivity field is the increase of number of defects in the crystal upon the introduction of Fe, which in turn reduces strongly the average distance between defects *l*.

The comparison of M_r of $Co_{2,25}Fe_{0,75}O_2BO_3$ with that of $Co_3O_2BO_3$, may now be done with the new measurements of the hysteresis cycles of the latter compound single crystal, since in Ref. 13 it could not be discerned whether their M_r data corresponded to a single crystal or a collection of crystals with different orientations. The value found is M_r = 3.4(1) μ_B/f.u., i.e. much larger than the previously published result, most probably because of the fact that our measurement was on an oriented single crystal. Besides, in the present work the remanent magnetization in the $Fe_3O_2BO_3$ *a* direction was found in the F phase to be $M_r(T$=65K) = 0.16 μ_B/f.u., similar to the average value previously published of 0.1 μ_B at 70 K [30], and drastically different from powder neutron diffraction [28] 2.36 μ_B/f.u. On the other hand, the value given for $Co_2FeO_2BO_3$ (0.48 μ_B/f.u.) [29,33] is half that found for $Co_{2,25}Fe_{0,75}O_2BO_3$ (0.9 μ_B/f.u.), although we explain this difference in the former compound as due to possible misorientation of the crystal in that paper. From this comparison a very puzzling conclusion is drawn. The effect of substitution of 25% of Co atoms by Fe is a dramatic decrease of M_r, which cannot be explained by Co moments (μ_{eff}=7.2 μ_B) being substituted by Fe ones (μ_{eff} =9.34 μ_B).

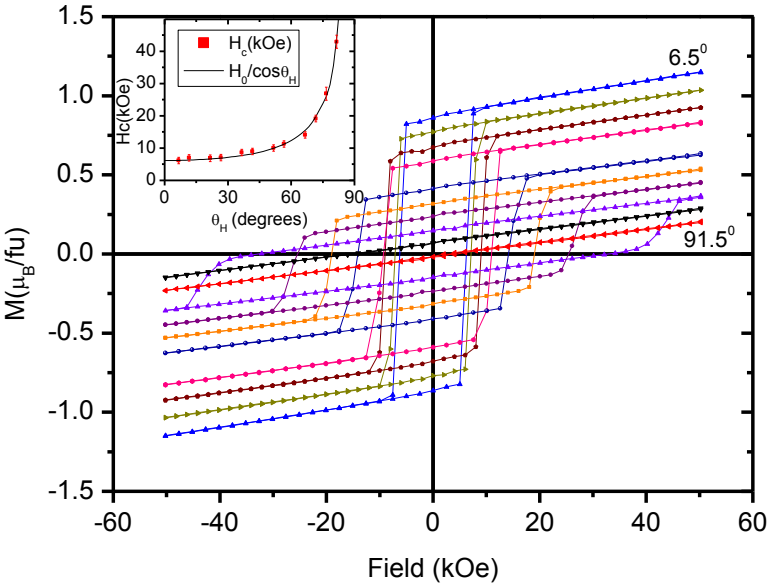

Fig.21. Hysteresis cycles of a $Co_{2.25}Fe_{0.75}O_2BO_3$ single crystal at T=50 K, as a function of rotation around the c axis. The extreme values θ_H are indicated. The inset shows the variation of $H_C$as a function of θ_H. The fit to a $1/cos\theta_H$ function is also shown.

It is important to estimate the expected values of the effective moment per formula unit in the paramagnetic phase for the considered set of ludwigite compounds to understand whether the orbital moments of magnetic ions are quenched or not. To analyze this question, first, the orbital component of magnetic moment is neglected and the spin component of the effective moment is calculated according with the formula: $\mu_S^2 = \sum_i g_i^2 S_i(S_i+1)$, accounting for the contribution of each type of transition ions. We assumed that all ions are in the high spin state and that in the mixed ludwigites all iron ions are in trivalent state. The spin values of magnetic ions are the next: (Co^{2+}: S=3/2, Co^{3+}:S=2, Fe^{2+}: S=2 and Fe^{3+}: S=5/2), g = 2. There are two divalent ions and one trivalent ion in formula unit. Then for $Co_3O_2BO_3$: $\mu_S = \sqrt{4\cdot\left(2\cdot\frac{3}{2}\left(\frac{3}{2}+1\right)+1\cdot 2(2+1)\right)} = 7{,}35\,\mu_B$

By analogy, for $Co_2FeO_2BO_3$: $\mu_S = \sqrt{4\cdot\left(2\cdot\frac{3}{2}\left(\frac{3}{2}+1\right)+1\cdot\frac{5}{2}\cdot(\frac{5}{2}+1)\right)} = 8{,}06\ \mu_B$ and for

$Fe_3O_2BO_3$: $\mu_S = \cdot\sqrt{4\left(2\cdot 2\cdot(2+1)+1\cdot\frac{5}{2}\cdot\left(\frac{5}{2}+1\right)\right)} = 9{,}11\,\mu_B$. These values shown in the Table 7 (Column 5). Secondly, we have tried to estimate the expected values of formula unit effective magnetic moment taking into account its orbital component. In this case $\mu_J^2 = \sum_i g_i^2 J_i(J_i+1)$. The scheme of Co ion electron levels is very sensitive to the crystal field and it is not available at present for all cases of distorted oxygen octahedra in ludwigite structure. Therefore, we have used the results of Z. Ropka and R.J. Radwansky [62], which have calculated electron levels energies and *g* values for different *J* for cobalt ions in $LaCoO_3$. According to them, we have assumed for high spin d^6 ions Co^{3+} and Fe^{2+}: J=1, g=3.4. For high spin d^7 ion Co^{2+} we assume J=1/2, g=2.21. And for d^5 ion Fe^{3+} it is clear that J=S=5/2 and g=2. The corresponding values of formula unit effective magnetic moment $\mu_J$are in the Table 7 (Column 6). Comparing the calculated values of μ_S and μ_J with the experimental value μ_{eff},one can see that the spin value $\mu_S$is closer to it than μ_J. So, we can conclude, that the orbital moments of Co and Fe ions are almost quenched.

One striking result of this work is the drastic reduction of magnetic moment in the *b* direction with respect to the $Co_3O_2BO_3$ compound. A naïve accounting of the magnetic moment per Co in $Co_3O_2BO_3$ yields $m_{Co\ atom}$=M_r/3=1.15 μ_B/Co along the *b* direction, therefore in $Co_{2.25}Fe_{0.75}O_2BO_3$ the Co sublattice should account for $m_{Co\ sublattice}$=2.58 μ_B, while the observed M_r=0.9 μ_B. The difference can be conjectured to be caused by the Fe moments being oriented with a component of the Fe sublattice m_{Fe}=1.68 μ_B(2.24 μ_B/Fe atom) opposing the net moment of the Co sublattice. Indeed, if the Fe moments order similarwise to $Fe_3O_2BO_3$, the moments at sites 2 and 4 would be oriented in the *b* direction and would tend to compensate one with each other, and would also oppose the Co magnetic moment in that direction. There should be an interplay of compensation of Co moments in the diluted compound and probably Fe-Co antiferromagnetic interactions to account for the reduction of M_r.

5.4 Spin-glass behavior of $Co_{1.7}Mn_{1.3}O_2BO_3$

The results of magnetic measurements are presented in the Fig. 22-24. Fig. 22 shows the ZFC and FC temperature magnetization behavior $M(T)$ in the fields 1 and 50 kOe. The first that catches the eye is the magnetic transition near T_N = 41 K, very close to the similar one in $Co_3O_2BO_3$. The next is the strongly pronounced splitting of ZFC and FC $M(T)$ dependencies below T_N. Despite the closeness of magnetic ordering temperatures in $Co_3O_2BO_3$ and $Co_{1.7}Mn_{1.3}O_2BO_3$ the type of magnetic ordering in these two compounds is obviously different. Instead of the ferromagnetic parent $Co_3O_2BO_3$, in the latter compound the most probable type of magnetic ordering is the spin-glass freezing. The magnetization curves $M(H)$ also evidence in favor of this proposal. In the ordered state $M(H)$ dependencies look as slightly open hysteresis loops with low remnant magnetization values (Fig. 23).

Assuming that the position 4 belongs to the trivalent ions and taking into account site occupation factors, one can write the valence formula of our mixed ludwigite as $Co^{2+}_{1.37}Mn^{2+}_{0.63}Co^{3+}_{0.35}Mn^{3+}_{0.65}(O_2BO_3)^{7-}$. Then the average effective magnetic moment per one transition ion can be calculated as

$$\mu_{\text{eff}} = g \cdot \sqrt{\frac{n^{2+}_{\text{Co}} \cdot \frac{3}{2} \cdot \frac{5}{2} + n^{2+}_{\text{Mn}} \cdot \frac{5}{2} \cdot \frac{7}{2} + (n^{3+}_{\text{Co}} + n^{3+}_{\text{Mn}}) \cdot 2 \cdot 3}{n}} .$$

Here n is a total number of magnetic ions in the formula unit. Accounting $n^{2+}_{\text{Co}} = 1.37$; $n^{2+}_{\text{Mn}} = 0.63$; $(n^{3+}_{\text{Co}} + n^{3+}_{\text{Mn}}) = 1$; $n = 3$, we get μ_{eff}= 4.71 μ_B, in a good agreement with the experimental value. Therefore, the magnetic data confirm the suggestion of closeness of Mn^{2+} and Mn^{3+} concentrations in our compound.

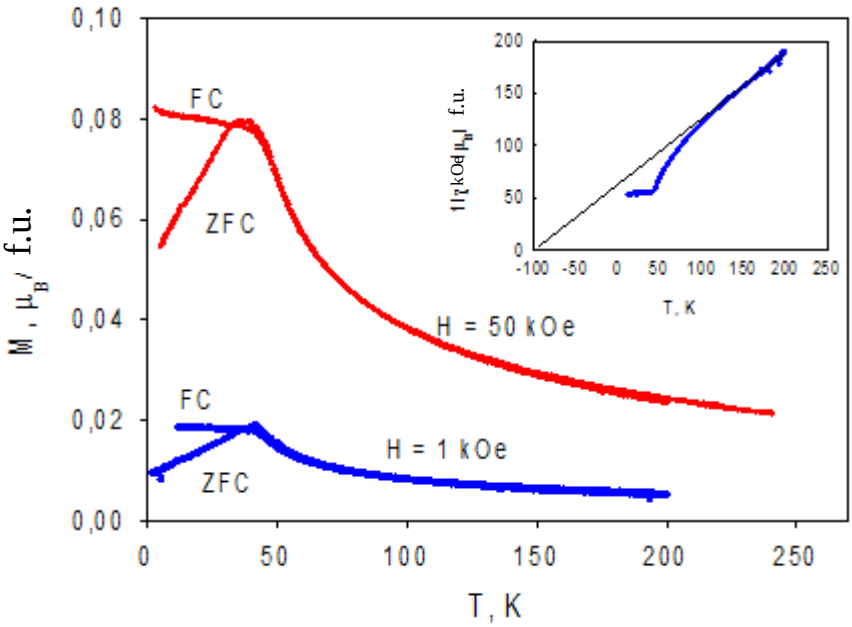

Figure 22. Field cooled (FC) and zero field cooled (ZFC) temperature magnetization dependences of $Co_{1.7}Mn_{1.3}O_2BO_3$ single crystal in the magnetic field *H*=1 and 50 kOe. The onset of the magnetic ordering is near 41 K.

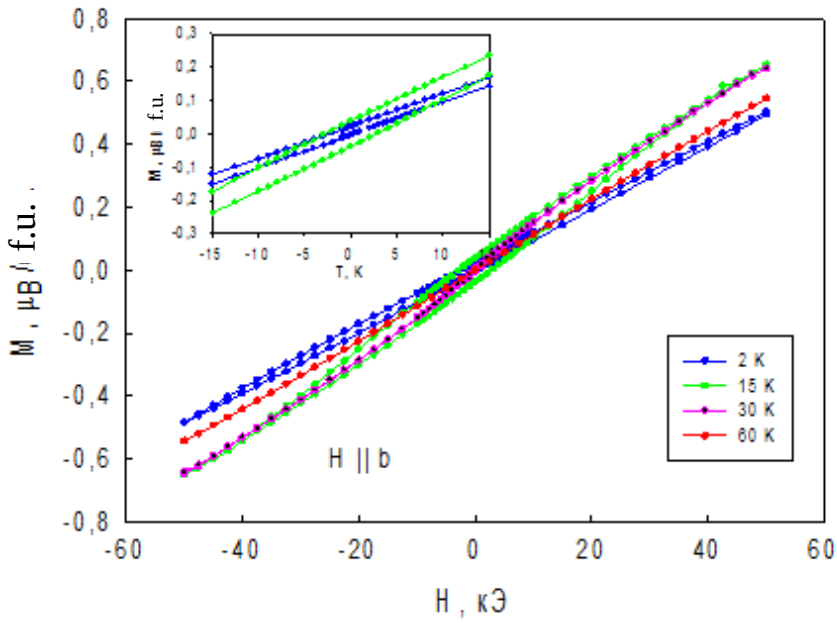

Fig. 23. Magnetization isotherms of $Co_{1.7}Mn_{1.3}O_2BO_3$.

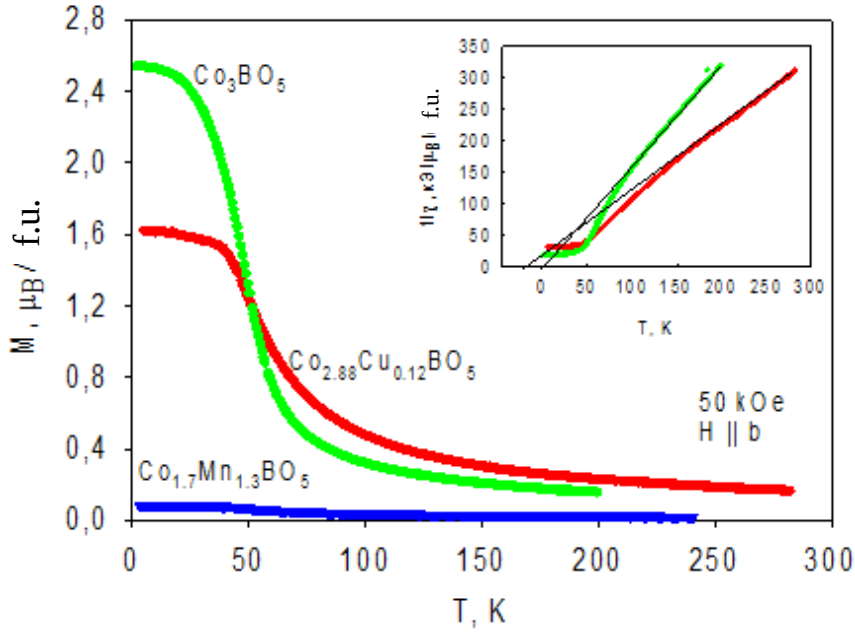

Fig. 24. Comparative representation of temperature dependencies of magnetization of Co_3BO_5, $Co_{1.7}Mn_{1.3}BO_5$ and $Co_{2.88}Cu_{0.12}BO_5$at 50 kOe magnetic field. The inset show the deviation of 1/χ from Curie-Weiss law.

At the temperatures above the magnetic transition, $Co_{1.7}Mn_{1.3}O_2BO_3$ shows the typical paramagnetic behavior. The inverse magnetic susceptibility temperature well obeys Curie-Weiss law at temperatures higher than 100 K (Fig. 24). The paramagnetic Curie temperature Θ = – 100 K is negative pointing out the predominance of antiferromagnetic interactions. The effective average magnetic moment per one magnetic ion is μ_{eff} = 4.83 μ_B (Table 8).

5.5 Magnetic properties of $Co_{2.88}Cu_{0.12}O_2BO_3$

The *dc*-magnetization has been measured as a function of temperature for two different values of magnetic field: 0.6 and 50 kOe. Fig.25 shows the FC and ZFC magnetization behavior for a 0.6 kOe field. The magnetization data show that the $Co_{2.88}Cu_{0.12}O_2BO_3$ ludwigite sample has a high magnetic anisotropy. The magnetic moment measured for a field directed along the *a* and *c* crystallographic axes was about 100 times smaller than that along the *b*-axis. These values are near the sensi-

tivity limit of the magnetometer. With the magnetometer used here, it is impossible to provide perfect coincidence of magnetic field direction with any crystallographic axis, so that a small projection of the magnetic moment along b could contribute to the measured signals for the a- and c-directions. For these reasons we ignore the a and c data and concentrate on the values of *M* measured with the magnetic field along the b-axis. These indicate that the magnetic transition occurs near T_C=43 K, the same as the critical temperature for unsubstituted $Co_3O_2BO_3$.

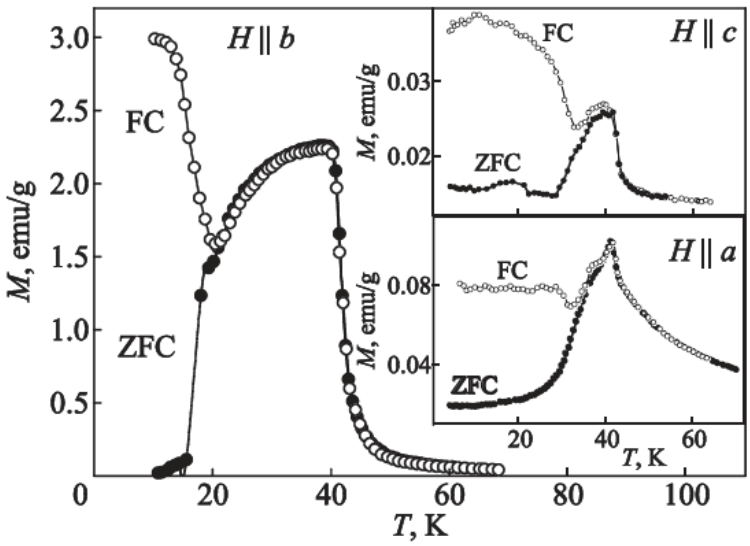

Fig. 25. FC and ZFC magnetization curves $Co_{2.88}Cu_{0.12}O_2BO_3$ in magnetic field 0.6 kOe

In the parent compound $Co_3O_2BO_3$ the magnetic transition is followed by a pronounced λ-anomaly in the heat capacity, which confirms its first order character. In $Co_{2.88}Cu_{0.12}O_2BO_3$ the magnetic transition in a 0.6 kOe field varies sharply with temperature which suggests that it is similar to the transition in $Co_3O_2BO_3$. The FC and ZFC dependences for H=0.6 kOe are very different at low temperatures. They diverge sharply at T_{div}=21 K, considerably below the magnetic transition temperature. This is not usually so in spin or cluster spin glasses [63].It seems that in the case of $Co_{2.88}Cu_{0.12}O_2BO_3$, by analogy with $Co_3O_2BO_3$, the divergence of the FC and ZFC curves is caused by the motion of domain walls, rather than by freezing of the magnetic moments.

Table 8. Collected magnetic transition temperature data for $Co_{1.7}Mn_{1.3}O_2BO_3$ and $Co_{2.88}Cu_{0.12}O_2BO_3$ in comparison with Co_3BO_5

	T_C , T_N, T_{SG} , K	*EMD*	μ_{eff}, μ_B/ f.u.	μ_S, μ_B/ f.u.	θ,K	M_r, μ_B/f.u..	χ_{AF}, μ_B/ f.u../Oe
Co_3BO_5	42	*b*	7.20	7.35	**1.2 (*b*) -154(*a*)**	**3.4**	$1.59\cdot10^{-6}$
$Co_{2.88}Cu_{0.12}BO_5$	**43**	***b***	**6.63**	**7.25**	**-12.6(*b*)**	**0.94**	$\mathbf{16.6}\cdot10^{-6}$
$Co_{1.7}Mn_{1.3}BO_5$	**41**	**–**	**8.15**	**8.36**	**-100**	**0.024**	$\mathbf{9.8}\cdot10^{-6}$

On the other hand, the M(T) measurements in a high (50 kOe) magnetic field indicate similar behavior of the FC and ZFC magnetizations (Fig. 24). In the paramagnetic phase at T > 150 K the inverse magnetic susceptibility temperature dependence (the inset to Fig. 24) obeys the Curie-Weiss law, quite well. The effective magnetic moment is μ_{eff} =3.83 μ_B calculated from the Curie constant C is slightly lower than that for $Co_3O_2BO_3$ (Table 8). The paramagnetic Curie temperature Θ = -12.6K indicates a weak predominance of antiferromagnetic interactions. Between 43 and 150 K, magnetic correlations cause the deviations from Curie-Weiss behavior.

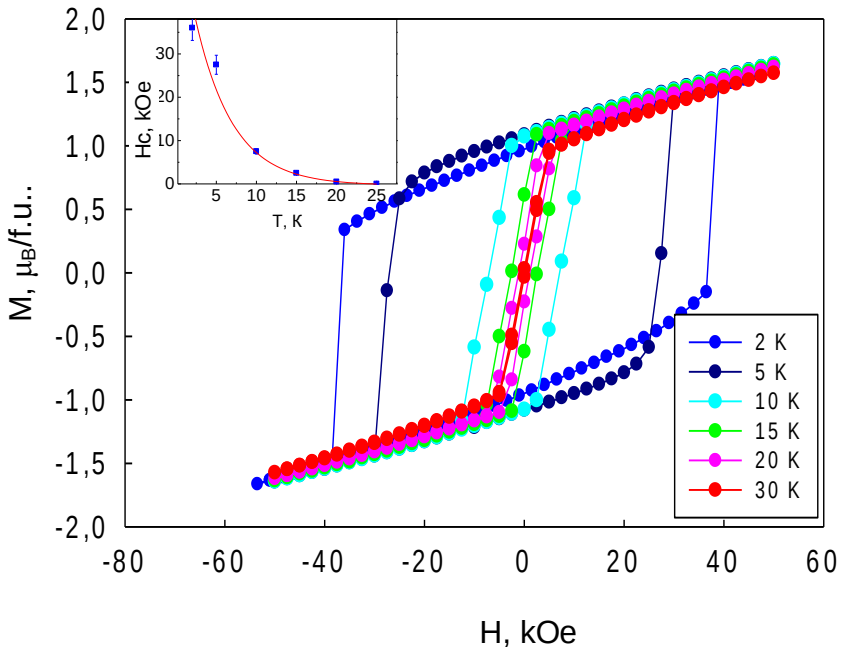

Fig. 26.The hysteresis loops corresponding to the magnetization isotherms of single crystal $Co_{2.88}Cu_{0.12}O_2BO_3$. The magnetic field is parallel to the *b*-axis

In the magnetically ordered phase, the magnetization curves show the appearance of hysteresis loops (Fig. 26). The loops are in the form of parallelograms, symmetric, with no shift relative the coordinate origin. The coercive field is almost 40 kOe at 2K and the remnant magnetization is close to 20 emu/g, which corresponds to 0.32 μ_B per magnetic ion. The maximum value of the magnetization for a magnetic field of 50 kOe is near 1.16 μ_B/ion, while the theoretical magnetic moment (spin only) value for $Co_3O_2BO_3$ is 3.3 μ_B /f.u. Thus, the experimental magnetic moment is far from the maximum possible value, which suggests partial compensation. The magnetization does not saturate up to H=50 kOe at any temperature. The high field branches of the loops are nearly linear, which indicates a possible antiferromagnetic contribution to the magnetic moment. The observed behavior of M(H) is very similar to that in the parent $Co_3O_2BO_3$.It seems that in both compounds the magnetic ordering at 43K is ferrimagnetic.

6. THEORETICAL STUDY OF LUDWIGITE MAGNETIC STRUCTURE

A theoretical study of the observed magnetic behavior of the samples was carried out according to the indirect exchange coupling model. The parameters of the electron transfer (*b*, *c*), the intra-atom exchange integral (*J*), and the ligand-cation electronic excitation energy (*U*) are used as the basic parameters in the model. Only the nearest metal-oxygen-metal neighbors (Me-O-Me) are taken into account. Relations with the next neighbors of the type Me-O-Me-O-Me are not taken into account in calculations. Complete expression of the exchange interaction is the sum of the integrals of the exchange over all individual orbits cation-ligand-cation.

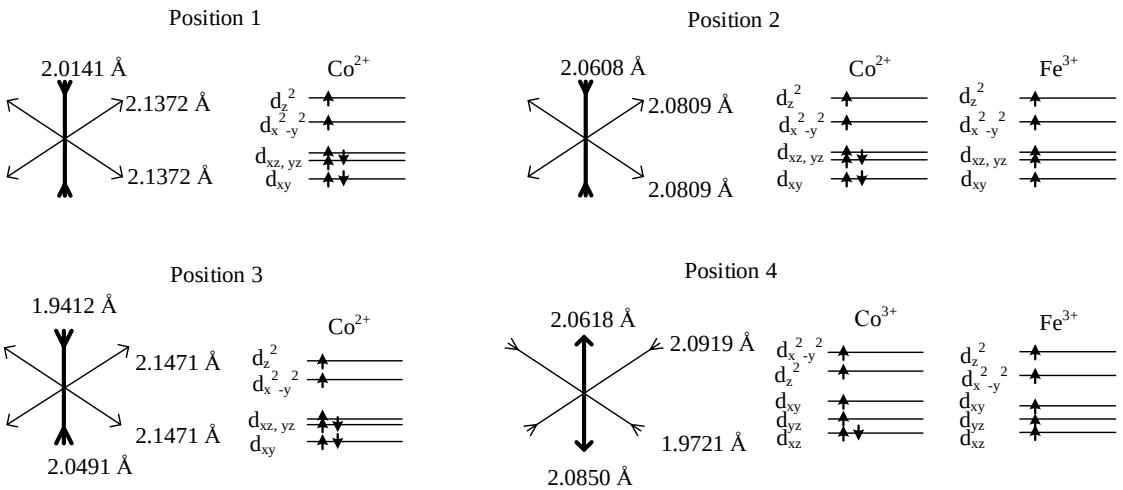

Fig.27. The scheme of electronic levels for Co^{2+}, Co^{3+} and Fe^{3+}in $Co_{2.25}Fe_{0.75}O_2BO_3$. The main octahedral axis shown by bold

The scheme of the energy levels for Co^{2+}, Co^{3+} and Fe^{3+}obtained from $Co_{2.25}Fe_{0.75}O_2BO_3$ single crystal with respect to local octahedral distortions and the population of nonequivalent positions, is shown in Fig. 27. In the ludwigite structure occur two types of exchange interactions: 90 ° and 180 ° indirect exchange interactions. In the latter case, the bond angle is taken into account by introducing cosΘ function. All the indirect interactions in the ludwigite structure are shown in Fig. 28. The composition and the number of bonds are identical for the investigated set of ludwigites. The interactions between the nearest ions

is carried out through the two common oxygen ions in a 90° character (*J*1, *J*3-*J*7, *J*9 and *J*11). For the *J*10 exchange, the angle between the interacting cations in positions 2 and 4 is 162°. The connection between the zigzag walls is carried out through a common oxygen atom with angles of 115 ° and 119 °, respectively.

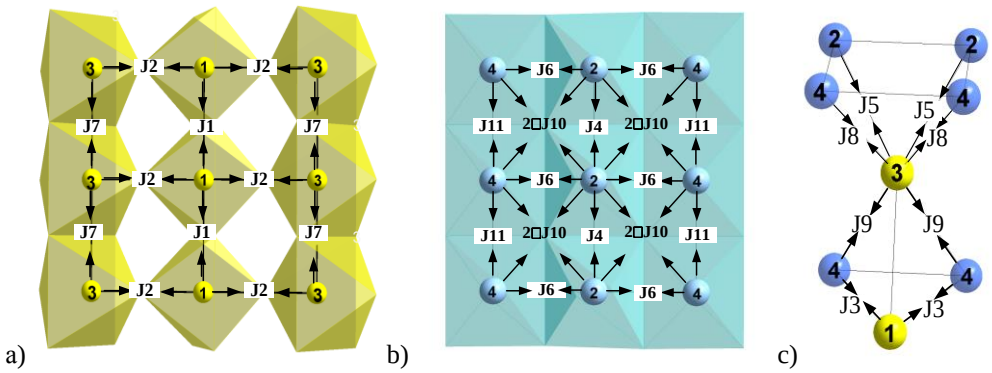

Fig. 28. Exchange interactions in spin ladder 3-1-3 (a), 4-2-4 (b) and between spin ladders (c).

6.1 Exchange interactions and magnetic structure of $Co_{3-x}Fe_xO_2BO_3$

We take into account the cation distribution and valence from X-ray data for the calculation of indirect exchange interactions. The calculation is performed on the assumption of a high-spin ion state (S_{Co}^{2+} = 3/2, S_{Co}^{3+} = 2, S_{Fe}^{2+} = 2 and S_{Fe}^{3+} = 5/2). Expressions for exchange integrals obtained for homometallic samples ($Co_3O_2BO_3$ and $Fe_3O_2BO_3$) and substituted ludwigite $Co_{2.25}Fe_{0.75}O_2BO_3$ are shown in Tables 9 and 10 respectively.

Table 9.Exchange integrals forms for $Co_3O_2BO_3$ and $Fe_3O_2BO_3$

	$Fe_3O_2BO_3$	$Co_3O_2BO_3$
*J*1	$\frac{1}{16}c\left[\left(\frac{16}{3}b\right)J_{Fe^{2+}}-2c\left(U_{Fe^{2+}}+U_{Fe^{2+}}\right)\right]$	$\frac{1}{9}c\left[\left(\frac{16}{3}b+\frac{3}{2}c\right)J_{Co^{2+}}-\frac{1}{2}c\left(U_{Co^{2+}}+U_{Co^{2+}}\right)\right]$
*J*2	$\frac{1}{16}c\left[-\left(\frac{16}{9}b^2+2c^2\right)\left(U_{Fe^{2+}}+U_{Fe^{2+}}\right)\right]\lvert\cos 115°\rvert$	$\frac{1}{9}c\left[\frac{3}{2}c^2J_{Co^{2+}}-\left(\frac{16}{9}b^2+\frac{1}{2}c^2\right)\left(U_{Co^{2+}}+U_{Co^{2+}}\right)\right]\lvert\cos 115°\rvert$
*J*3	$\frac{1}{20}c\left[-\left(\frac{16}{3}b+c\right)\left(U_{Fe^{2+}}+U_{Fe^{2+}}\right)+cJ_{Fe^{2+}}\right]$	$\frac{1}{12}c\left[-\left(\frac{24}{6}b+\frac{1}{2}c\right)\left(U_{Co^{2+}}+U_{Co^{3+}}\right)+\left(\frac{8}{6}b+\frac{3}{2}c\right)J_{Co^{2+}}\right]$

	$Fe_3O_2BO_3$	$Co_3O_2BO_3$
*J*4	$\frac{1}{16}c\left[\left(\frac{16}{3}b\right)J_{Fe^{2+}}-2c\left(U_{Fe^{2+}}+U_{Fe^{2+}}\right)\right]$	$\frac{1}{9}c\left[\left(\frac{16}{3}b+\frac{3}{2}c\right)J_{Co^{2+}}-\frac{1}{2}c\left(U_{Co^{2+}}+U_{Co^{3+}}\right)\right]$
*J*5	$\frac{1}{16}c\left[2cJ_{Fe^{2+}}-\left(\frac{16}{3}b\right)\left(U_{Fe^{2+}}+U_{Fe^{2+}}\right)\right]$	$\frac{1}{9}c\left[\left(\frac{24}{6}b+\frac{1}{2}c\right)J_{Co^{2+}}-\left(\frac{8}{6}b+\frac{3}{2}c\right)\left(U_{Co^{2+}}+U_{Co^{2+}}\right)\right]$
*J*6	$\frac{1}{20}c\left[\left(\frac{8}{3}b\right)J_{Fe^{2+}}-\left(\frac{8}{3}b+2c\right)\left(U_{Fe^{2+}}+U_{Fe^{3+}}\right)\right]$	$\frac{1}{12}c\left[\left(\frac{8}{3}b+\frac{1}{2}c\right)J_{Fe^{2+}}-\left(\frac{8}{3}b+\frac{3}{2}c\right)\left(U_{Fe^{2+}}+U_{Fe^{3+}}\right)\right]$
*J*7	$\frac{1}{16}c\left[\left(\frac{16}{3}b\right)J_{Fe^{2+}}-2c\left(U_{Fe^{2+}}+U_{Fe^{2+}}\right)\right]$	$\frac{1}{9}c\left[\left(\frac{16}{3}b+\frac{3}{2}c\right)J_{Co^{2+}}-\frac{1}{2}c\left(U_{Co^{2+}}+U_{Co^{2+}}\right)\right]$
*J*8	$\frac{1}{20}\left[-\left(\frac{16}{9}b^2+2c^2\right)\left(U_{Fe^{2+}}+U_{Fe^{3+}}\right)\right]\lvert\cos 119°\rvert$	$\frac{1}{12}\left[c^2J_{Co^{2+}}-\left(\frac{16}{9}b^2+c^2\right)\left(U_{Co^{2+}}+U_{Co^{3+}}\right)\right]\lvert\cos 119°\rvert$
*J*9	$\frac{1}{20}c\left[cJ_{Fe^{2+}}-\left(\frac{16}{3}b+c\right)\left(U_{Fe^{2+}}+U_{Fe^{3+}}\right)\right]$	$\frac{1}{12}c\left[2cJ_{Co^{2+}}-\frac{16}{3}b\left(U_{Co^{2+}}+U_{Co^{3+}}\right)\right]$
*J*10	$\frac{1}{12}\left[c^2J_{Fe^{2+}}-\left(\frac{16}{9}b^2+c^2\right)\left(U_{Fe^{2+}}+U_{Fe^{3+}}\right)\right]\lvert\cos 162°\rvert$	$\frac{1}{12}\left[2c^2J_{Co^{2+}}-\frac{16}{9}b^2\left(U_{Co^{2+}}+U_{Co^{3+}}\right)\right]\lvert\cos 163°\rvert$
*J*11	$-\frac{1}{25}c\left[\left(\frac{16}{3}b+2c\right)\left(U_{Fe^{3+}}+U_{Fe^{3+}}\right)\right]$	$\frac{1}{16}c\left[\left(\frac{16}{3}b+2c\right)\left(U_{Co^{3+}}+U_{Co^{3+}}\right)\right]$

Table 10. Exchange integrals forms for $Co_3O_2BO_3$ and $Fe_3O_2BO_3$ $Co_{2,25}Fe_{0,75}O_2BO_3$

	$Co_{2,25}Fe_{0,75}O_2BO_3$
*J*1	$\frac{1}{9}c\left[\left(\frac{16}{3}b+\frac{3}{2}c\right)J_{Co^{2+}}-\frac{1}{2}c\left(U_{Co^{2+}}+U_{Co^{2+}}\right)\right]$
*J*2	$\frac{1}{9}c\left[\frac{3}{2}c^2J_{Co^{2+}}-\left(\frac{16}{9}b^2+\frac{1}{2}c^2\right)\left(U_{Co^{2+}}+U_{Co^{2+}}\right)\right]\lvert\cos 119°\rvert$
*J*3	$0,48\cdot\frac{1}{12}c\left[-\left(\frac{8}{3}b+\frac{1}{2}c\right)\left(U_{Co^{2+}}+U_{Co^{2+}}\right)-\left(\frac{8}{3}b+\frac{3}{2}c\right)J_{Co^{2+}}\right]+$ $\frac{0,54}{15}c\left[-\left(\frac{12}{3}b+\frac{1}{2}c\right)\left(U_{Co^{2+}}+U_{Fe^{3+}}\right)+\left(\frac{4}{3}b+\frac{3}{2}c\right)J_{Co^{2+}}\right]$
*J*4	$+\frac{0,14\cdot 0,14}{25}c\left[-\left(\frac{16}{3}b+2c\right)\left(U_{Fe^{3+}}+U_{Fe^{3+}}\right)\right]\Bigg]+$ $\frac{0,86\cdot 0,86}{9}c\left[\left(\frac{16}{3}b+\frac{3}{2}c\right)J_{Co^{2+}}-\left(\frac{1}{2}c\right)\left(U_{Co^{2+}}+U_{Co^{2+}}\right)\right]$ $2\frac{0,86\cdot 0,14}{15}\left[\left(\frac{8}{3}b+\frac{1}{2}c\right)J_{Co^{2+}}-\left(\frac{8}{3}b+\frac{3}{2}c\right)\left(U_{Fe^{3+}}+U_{Fe^{3+}}\right)\right]\Bigg]$
*J*5	$\frac{0,86}{9}c\left[\left(\frac{27}{6}b+c\right)J_{Co^{2+}}-\left(\frac{5}{6}b+c\right)\left(U_{Co^{2+}}+U_{Co^{2+}}\right)\right]+$

	$Co_{2,25}Fe_{0,75}O_2BO_3$
	$\frac{0,14}{15}c\left[\left(\frac{4}{3}b+\frac{1}{2}c\right)J_{Co^{2+}}-\left(\frac{12}{3}b+\frac{3}{2}c\right)\left(U_{Co^{2+}}+U_{Fe^{3+}}\right)\right]$
*J*6	$\frac{0,86\cdot 0,54}{15}c\left[\left(\frac{8}{3}b+c\right)J_{Co^{2+}}-\left(\frac{8}{3}b+c\right)\left(U_{Co^{2+}}+U_{Fe^{3+}}\right)\right]+$ $\frac{0,86\cdot 0,48}{12}c\left[\left(\frac{4}{3}b+c\right)J_{Co^{2+}}-\left(\frac{12}{3}b+c\right)\left(U_{Co^{2+}}+U_{Co^{3+}}\right)\right]$ $-\frac{0,14\cdot 0,48}{25}c\left[\left(\frac{16}{3}b+2c\right)\left(U_{Fe^{3+}}+U_{Fe^{3+}}\right)\right]-\frac{0,48\cdot 0,14}{20}c\left[\left(\frac{16}{3}b+2c\right)\left(U_{Co^{3+}}+U_{Fe^{3+}}\right)\right]$
*J*7	$\frac{1}{9}c\left[\left(\frac{16}{3}b+\frac{3}{2}c\right)J_{Co^{2+}}-\frac{1}{2}c\left(U_{Co^{2+}}+U_{Co^{2+}}\right)\right]$
*J*8	$\frac{0,54}{15}\left[cJ_{Co^{2+}}-\left(\frac{16}{9}b^2+c^2\right)\left(U_{Co^{2+}}+U_{Fe^{3+}}\right)\right]\lvert\cos 118°\rvert$ $+\frac{0,48}{12}\left[cJ_{Co^{2+}}-\left(\frac{16}{9}b^2+c^2\right)\left(U_{Co^{2+}}+U_{Co^{3+}}\right)\right]\lvert\cos 118°\rvert$
*J*9	$\frac{0,48}{12}c\left[\left(\frac{21}{6}b+c\right)J_{Co^{2+}}-\left(\frac{11}{6}b+c\right)\left(U_{Co^{2+}}+U_{Co^{3+}}\right)\right]+$ $\frac{0,54}{15}c\left[\left(\frac{3}{3}\mathrm{b}+\mathrm{c}\right)J_{Co^{2+}}-\left(\frac{13}{3}\mathrm{b}+\mathrm{c}\right)\left(U_{Co^{2+}}+U_{Fe^{3+}}\right)\right]$
*J*10	$\frac{0,86\cdot 0,54}{15}\left[\frac{1}{2}c^2J_{Co^{2+}}-\left(\frac{16}{9}b^2+\frac{3}{2}c^2\right)\left(U_{Co^{2+}}+U_{Fe^{3+}}\right)\right]\lvert\cos 164°\rvert$ $+\frac{0,86\cdot 0,48}{12}\left[\frac{1}{2}cJ_{Co^{2+}}-\left(\frac{16}{9}b^2+\frac{3}{2}c^2\right)\left(U_{Co^{2+}}+U_{Co^{3+}}\right)\right]\lvert\cos 164°\rvert$ $+\frac{0,48\cdot 0,14}{20}\left[c^2J_{Co^{2+}}-\left(\frac{16}{9}b^2+c^2\right)\left(U_{Co^{3+}}+U_{Fe^{3+}}\right)\right]\lvert\cos 164°\rvert$ $-\frac{0,14\cdot 0,48}{25}\left[\left(\frac{16}{9}b^2+2c^2\right)\left(U_{Fe^{3+}}+U_{Fe^{3+}}\right)\right]\lvert\cos 164°\rvert$
*J*11	$\frac{1}{25}c\left[-\left(\frac{16}{3}b+2c\right)\left(U_{Fe^{3+}}+U_{Fe^{3+}}\right)\right]+\frac{1}{20}c\left[c^2J_{Co^{3+}}-\left(\frac{16}{3}b+c\right)\left(U_{Co^{3+}}+U_{Fe^{3+}}\right)\right]+$ $\frac{1}{16}c\left[c^2J_{Co^{3+}}-\left(\frac{16}{3}b+c\right)\left(U_{Co^{3+}}+U_{Co^{3+}}\right)\right]$

Table 11 lists the model parameters for each type of magnetic ion [64]. The obtained values of the exchange integrals sre shown in Table 12. Using this meth-

od,we are able to determine only the mutual orientation of the magnetic moments in the structure, but for the complete analysis of the magnetic structure and comparison with the experimental data, the spatial orientation of the magnetic moments relative to the single-crystal axes is required. Theoretical group analysis [65] showed that possible directions of the magnetic moments for the low-temperature phase of $Fe_3O_2BO_3$ (the spatial group *Pbnm* (62)): position 1 – [100]; 2–$[0\bar{1}0]$, [010], 3 – $[\bar{1}00]$, 4 – [010], $[0\bar{1}0]$. For a ferrimagnetic state in Co-containing ludwigites (spatial group *Pbam* (55)), this analysis yields the following results:

1) 1 – [010], 2 – [010], 3 – $[0\bar{1}0]$и 4 –$[0\bar{1}0]$;

2) 1 – [010], 2 –$[0\bar{1}0]$, 3 – $[0\bar{1}0]$и 4 – [010].

Table11. Indirect exchange model parameters for cations

	Co^{2+}	Co^{3+}	Fe^{2+}	Fe^{3+}	Mn^{2+}	Mn^{3+}	Cu^{2+}
J_{Me}, eV	2.5	2.5	3.0	3.0	3.0	3.0	1.8
U_{Me}, eV	3.2	3.8	4.0	4.5	4.5	5.2	3.0
b	0.02						
c	0.01						

As can be seen from Table 12, most interactions have an antiferromagnetic character. Ferromagnetic interactions are between Me^{2+} ions at positions 1-1, 2-2, and 3-3 (*J*1, *J*4 and *J*7). Cobalt enhances the ferromagnetic contribution. The case of $Fe_3O_2BO_3$ the most intense exchange are*J*3, *J*9 and *J*11 and *J*5. *J*1, *J*2 and *J*7 present the interactions inside the spin ladder 3-1-3 (Fig.28a), *J*4, *J*6, *J*10 and *J*11 are the interactions inside the spin ladder 4-2-4 (Fig.28b) .The integrals *J*3, *J*5 , *J*8 and *J*9 describe inter-wall interactions (Fig.28c).

Cations 1 and 3 are connected to each other via oxygen atoms in the octahedron vertex. Thus, the magnetic ions in the spin ladder 3-1-3 are located at the nodes of the square lattice without diagonal bonds. Positive interactions *J*1 and *J*7 form infinite ferromagnetic chains 1-1 and 3-3 along the *c*-axis. The interactions between

the chains are antiferromagnetic and form a collinear spin structure. This coincides with the experimentally observed neutron diffraction data in $Fe_3O_2BO_3$ (antiferromagnetically bound ferromagnetic chains along the *c*-axis) [27,28].

Table12.Exchange integrals value (K) for $Co_{3-x}Fe_xO_2BO_3$ (x = 0,0; 0,75; 3,0). Frustrated interactions indicated in italic. Intense ordered interactions – by bold.

	$Fe_3O_2BO_3$	$Co_{2.25}Fe_{0.75}O_2BO_3$	$Co_3O_2BO_3$
*J*1	**+1.16**	**+3.5**	**+3.5**
*J*2	**-2.64**	**-3.53**	**-2.89**
*J*3	*-5.38*	*-5.05*	*-4.51*
*J*4	*+1.16*	*+1.02*	**+3.5**
*J*5	*-5.70*	*+0.48*	**+1.0**
*J*6	*-2.29*	*-3.8*	**-2.42**
*J*7	**+1.16**	**+3.5**	**+3.5**
*J*8	*-2.58*	*-2.18*	**-2.44**
*J*9	*-5.54*	*-4.64*	**-2.4**
*J*10	**-3.58**	**-4.23**	**-4.23**
*J*11	**-5.29**	**-5.29**	*-5.45*

In the spin ladder 4-2-4, the exchange interactions between all cations formed through the octahedral common edges, which leads to the appearance of an additional diagonal interaction *J*10. The interactions *J*10, *J*11 determine the ordering in the stairs 4-2-4 and form the infinite ferromagnetic-coupled antiferromagnetic chains 2-2 and 4-4 along the *c*-axis. This was confirmed by neutron diffraction experiment [28].

All the exchange interactions between the stairs in $Fe_3O_2BO_3$ are antiferromagnetic. The interactions between the ladders are *J*3 and *J*5, *J*8 and *J*9. Ions 1-4-4 form a distorted triangular lattice. Thus, interactions are negative and have close magnitudes: $J3 = J3 \approx J11 \approx -5.3$ K. This leads to frustration of the J3 interactions (Fig. 29b).

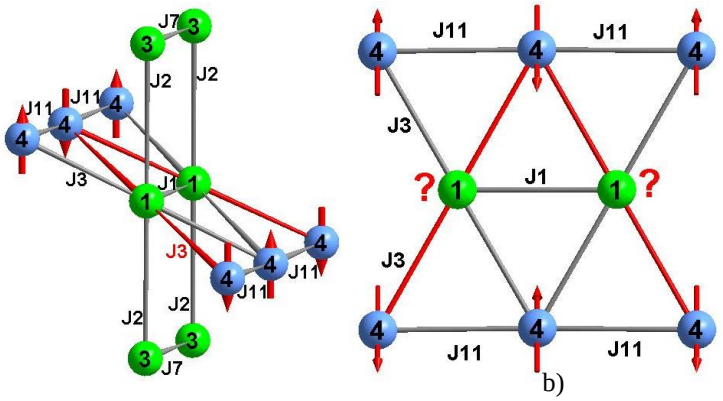

a) b)

Fig.29. Interladder exchange interactionsin $Fe_3O_2BO_3$ via Position 1. Frustrated interactions indicated by red color.a) Frustrated and ordered Interladder interactions*J*1, *J*2 *J*3. б) Triangle magnetic lattice with ambiguously spin orientation in position 1.

The magnetic ions in position 3 are at the apex of the two pyramids (Fig. 30). The triangular faces of the pyramids also lead to frustrations. As a result, the magnetic structure of $Fe_3O_2BO_3$ is divided into two independent orthogonal subsystems, which was found experimentally. In fact, due to frustrations, the exchange interactions between the ladders are compensated, and the ordering in the stairs 4-2-4 and 3-1-3 occurs independently of each other.

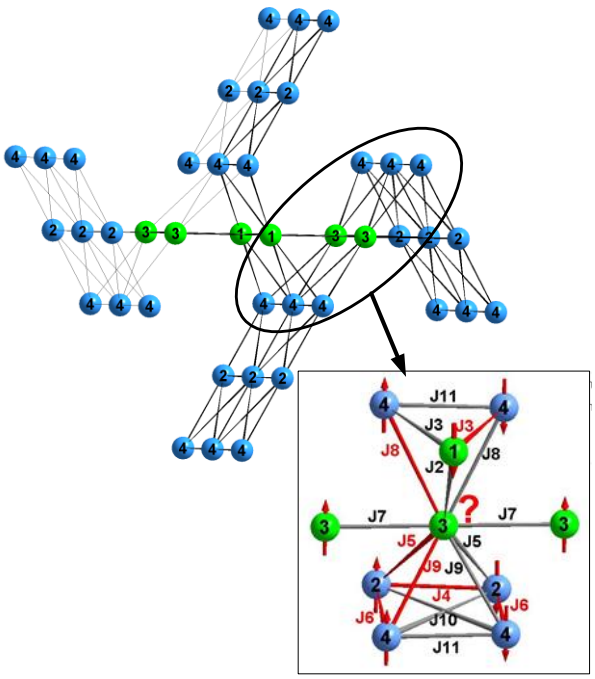

Fig.30.Interladder exchange interactions in $Fe_3O_2BO_3$ via cation position 3. Frustrated interactions indicated by red color.

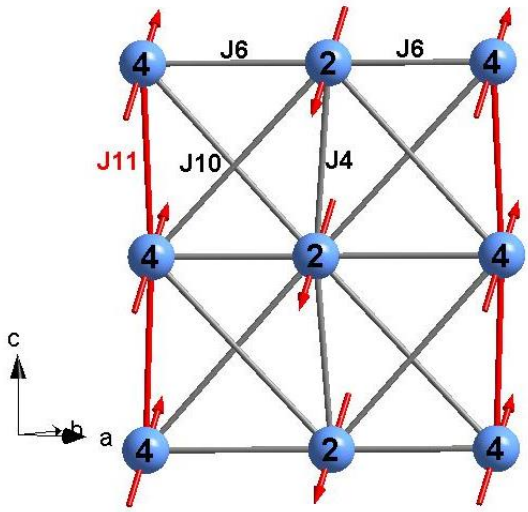

Fig.31.Exchange interactions in ladder 4-2-4 в $Co_3O_2BO_3$. Тёмнымвыделенаfrustrated interactions indicated by red color

As a result, magnetic chains appear along the *c*-axis with a strong antiferromagnetic coupling, which is accompanied by a doubling of the magnetic cell along the *c*-axis. This was found in neutron diffraction studies [27,28]. Thus, the proposed model reproduces the experimental features of the magnetic behavior of $Fe_3O_2BO_3$.

Increase in the electron population of the Co t_{2g}-level in $Co_3O_2BO_3$ leads to an increase in the ferromagnetic contribution. The interaction between ions in positions 2 and 3 changes its sign (from $J5$ = -5.7 K in $Fe_3O_2BO_3$ to +1.0 K in $Co_3O_2BO_3$). This stabilizes the collinear structure (Fig. 31). Such a configuration is possible from the point of view of theoretical-group analysis, according to which the interaction inside the 4-4 chain is ferromagnetic [65]. The ordering in 4-2-4 is antiferromagnetic, and between the stairs is ferromagnetic.

This does not lead to frustrations between the ladders (Figure 32 b). In positions 2 and 3, all exchange interactions are of ordering type and enhance the connection between the ladders, which facilitates the establishment of long-range magnetic order in the sample.

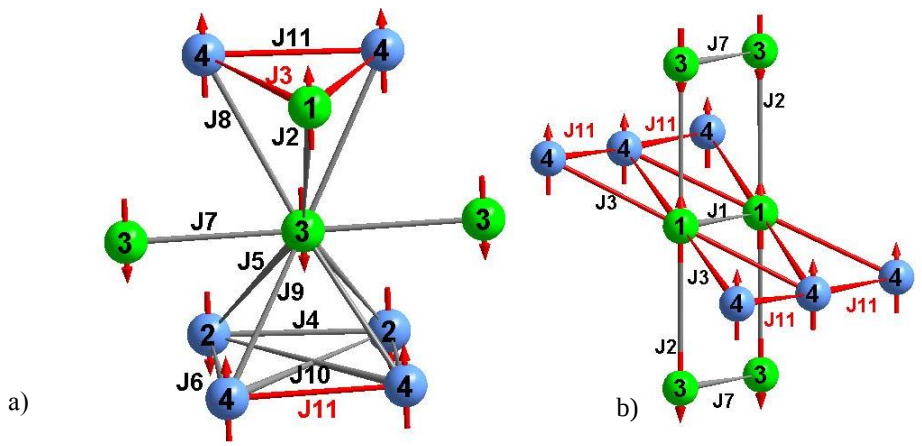

Fig.32.Interladder exchange interactions in $Co_3O_2BO_3$via cation position 3 (a) and 1 (b). Frustrated interactions indicated by red color.

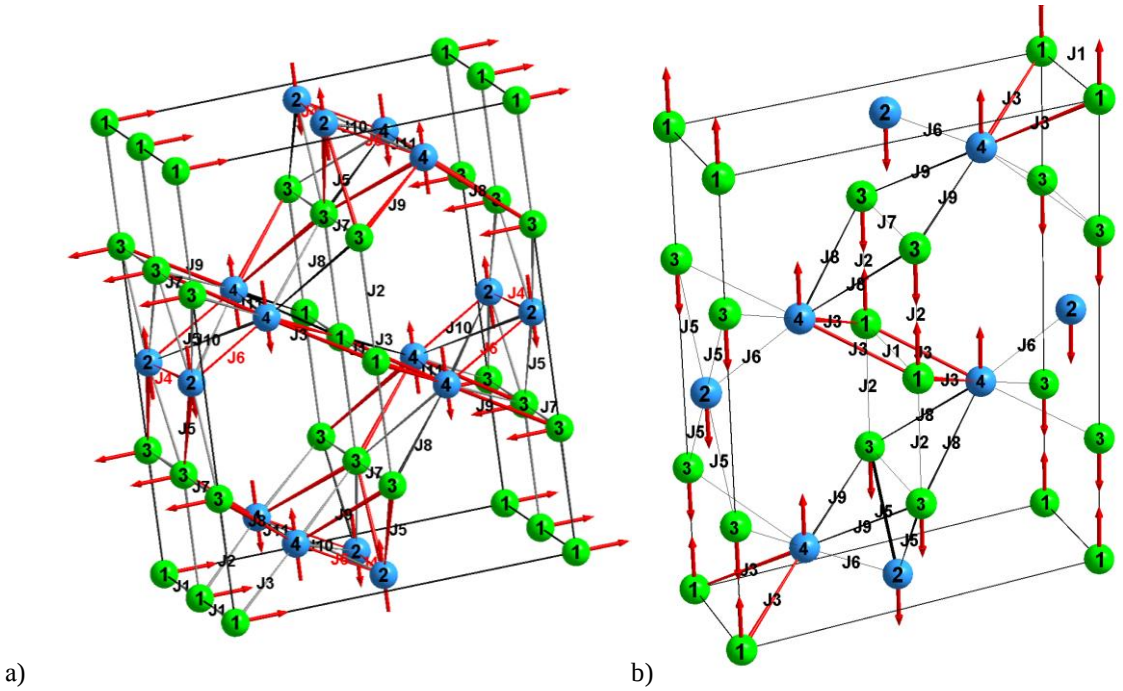

Fig. 33. Proposed magnetic structure of a) $Fe_3O_2BO_3$, b) $Co_3O_2BO_3$.
Nonequivalent crystallographic positions indicated by numbers
Frustrated interactions indicated by red color.

In ludwigite structure there is a certain critical level of magnetic frustrations, below which the long-range order throughout the sample is most preferable. This is implemented in $Co_3O_2BO_3$. Calculation of the temperature of the magnetic transition in $Co_3O_2BO_3$ by the indirect exchange coupling model yields T_C = 46 K, which well agrees with the experimental data.

Pattern of exchange interactions in $Co_{2.25}Fe_{0.75}O_2BO_3$ is most similar to $Fe_3O_2BO_3$. The nature of the interactions in the triads 4-2-4 and 3-1-3 is conserved, which leads to the establishment of an antiferromagnetic order at T_N = 115 K and a ferrimagnetic order at T_C = 70 K.

The complex study with the method of calculating indirect exchange interactions and calculating possible magnetic structures, in accordance with theoretical group analysis, makes it possible to construct a local magnetic structure of the $Fe_3O_2BO_3$ and $Co_3O_2BO_3$ with the orientation of the magnetic moments of the cations relative to the crystallographic axes of single crystals (Fig. 33).

6.2 Exchange interactions in $Co_{2,88}Cu_{0,12}O_2BO_3$ and $Co_{1,7}Mn_{1,3}O_2BO_3$

The results of the exchange interactions calculation in Cu- and Mn-doped ludwigites given in Table 13. Earlier, the presence of frustrating interactions (*J*8 and *J*9) in the structure was demonstrated using the example of $Cu_2FeO_2BO_3$ [36]. The effects of magnetic frustrations and cationic disorder in this ludwigite lead to the establishment of a spin glass state at 63 K [6]. The investigation of the exchange interactions of the $Co_{2,88}Cu_{0,12}O_2BO_3$ demonstrated that a small amount of copper does not lead to appreciable changes in the magnetic structure compared to $Co_3O_2BO_3$.

The decrease in the exchange interactions (*J*6, *J*11) is connected to the Cu-substitution in position 4. The calculated temperature of the magnetic transition in $Co_{2.88}Cu_{0.12}O_2BO_3$ is T_C = 39 K and close to the experimental value (T_C= 43 K).

Probably, the combination of cationic disorder and competition of exchange interactions is the cause of the spin-glass state in $Co_{1.7}Mn_{1.3}$ O_2BO_3. A characteristic feature of disordered systems is the presence of randomly changing pair interactions of atoms. The valence state of cobalt and manganese ions in $Co_{1.7}Mn_{1.3}$ O_2BO_3 are two- and trivalent states respectively. Because of this cationic disorder and fluctuations in the interatomic distances, the exchange interactions that determine the mutual orientation of the magnetic moments will randomly vary from one pair of atoms

to another. All interactions have an antiferromagnetic character, but their magnitude can vary several times, for example, *J*6, *J*10, *J*11

Table 13. Calculated exchange interactions for$Co_{2,88}Cu_{0,12}O_2BO_3$ and $Co_{1,7}Mn_{1,3}O_2BO_3$. Frustrated interactions indicated in italic. Powerful ordered interactions – by bold.

	Pos.	$Co_3O_2BO_3$	$Co_{2.88}Cu_{0.12}O_2BO_3$	$Co_{1.7}Mn_{1.3}O_2BO_3$
*J*1	1-1	**+3.5**	**+3.5**	**+2.92**
*J*2	1-3	**-2.89**	**-2.89**	**-1.91**
*J*3	1-4	*-4.5*	*-4.73*	*-5.82*
*J*4	2-2	**+3.5**	**+3.5**	+1.90
*J*5	2-3	*+1.88*	*+1.88*	*+1.59*
*J*6	2-4	**-1.97**	**-0.76**	**-3.47**
*J*7	3-3	**+3.5**	**+3.5**	+1.92
*J*8	3-4	*-2.44*	*-2.22*	*-2.35*
*J*9	3-4	*-2.44*	*-2.12*	*-6.78*
*J*10	2-4	**-4.23**	**-4.45**	**-2.27**
*J*11	4-4	*-5.45*	*-4.49*	*-4.44*

It was shown that cation substitution could lead to critical changes in the magnetic behavior of the system. The influence of cationic disorder multiplied by frustrated interactions can lead to a loss of long-range magnetic order, which is observed in $Co_{1.7}Mn_{1.3}O_2BO_3$ as a transition to the spin-glass state at T_{SG} = 41 K. However, if substitution occurs without the occurrence of cationic disorder, the magnetic properties of the system do not change ($Co_{2.88}Cu_{0.12}O_2BO_3$).

The degree of frustrations, as well as cationic disorder, have a critically important effect on the establishment of long-range magnetic order in $Co_3O_2BO_3$ and $Co_{2.88}Cu_{0.12}O_2BO_3$, or, conversely, the impossibility of the system to reach an ordered state in $Co_{1.7}Mn_{1.3}O_2BO_3$. This indicates a fine balance of exchange interactions in the structure of ludwigite.

SUMMARY

A complex study of substituted ludwigites has shown that cation substitution plays an important role in the formation of the magnetic properties of these materials. Within the framework of the indirect exchange model, an interpretation of the experimentally observed magnetic behavior is proposed. The most significant are the following results:

1. The crystal structure study of the ludwigites $Co_3O_2BO_3$, $Co_{2.25}Fe_{0.75}O_2BO_3$, $Co_{1.7}Mn_{1.3}O_2BO_3$, $Co_{2.88}Cu_{0.12}O_2BO_3$ determined spatial symmetry groups, parameters of elementary cells, coordinates of atoms, lengths and angles of interatomic bonds. The cation distribution over nonequivalent crystallographic positions was studied depending on the type and concentration of substitution cations.

2. Using the empirical BVS-method, the valence states of the cations were determined. From the calculation of the electric field gradient the nature and degree of coordination octahedra distortion was obtained.

3. The Mössbauer spectra were measured.The temperature dependences of hyperfine parameters in $Co_{2.25}Fe_{0.75}O_2BO_3$ were determined. A magnetic phase transition was found in the spin-ladder 4-2-4 at T_{N1} = 115 K.

4. Temperature, field and angular dependences of the static magnetization and dynamic magnetic susceptibility were measured. The temperature of magnetic phase transitions and the type of magnetic anisotropy were determined for all samples. A temperature-induced change in the easy axis of magnetization in $Fe_3O_2BO_3$ was observed. In $Co_{2.25}Fe_{0.75}O_2BO_3$, an extraordinary magnetic hardness was detected (up to 90 kOe). In $Co_{1.7}Mn_{1.3}O_2BO_3$ a transition to the spin-glass state was observed.

5. In terms of the indirect exchange model, we carried out the calculation of the exchange integrals. The scale of ordering and frustrating interactions was determined. The analysis of intra- and inter-chain exchange interactions were carried out. A model of the magnetic structure of $Fe_3O_2BO_3$ as a system of two weakly coupled orthogonal subsystems was proposed.

REFERENCES

[1]. Irwin, MICHAEL B., and RONALD C. Peterson. "The crystal structure of ludwigite." *Canadian mineralogist* 37 (1999): 939-944.

[2]. Appel, P. W. U., and M. F. Brigatti. "Ludwigite from central Sweden: new data and crystal structure refinement." *Mineralogical Magazine* 63.4 (1999): 511-511

[3]. Akhmanova, M. V. "The use of infrared (IR) spectra to study the structures of natural borates." *Zhurnal Strukturnoi Khimii* 3 (1962): 28-34.

[4]. Plyusnina, I. I., and Yu A. Kharitonov. "Crystallochemical properties and infrared absorption spectra of borates and borosilicates." *Journal of Structural Chemistry* 4.4 (1963): 506-516.

[5]. Aleksandrov, S. M., and M. A. Troneva. "Composition and genesis of endogenous borates from the Pitkáranta ore field, Karelia." *Geochemistry International* 47.9 (2009): 914-929.

[6]. Continentino, M. A., et al. "Magnetic interactions in the monoclinic ludwigite Cu FeO BO." *The European Physical Journal B-Condensed Matter and Complex Systems* 9.4 (1999): 613-618.

[7]. Utzolino, A., and K. Bluhm. "Synthesis and Characterization of Two New Compounds with Ludwigite-Structure: Co5Sn (BO3) 2O4 and Co5Mn (BO3) 2O4." *ChemInform* 27.27 (1996).

[8]. Bluhm, K., and Hk Müller-Buschbaum. "Ein Beitrag über Oxometallate mit trigonal planaren BO_3-Polyedern Ni_2MBO_5 (M= Ga, Fe, Al, Cr)." *Zeitschrift für anorganische und allgemeine Chemie* 582.1 (1990): 15-20.

[9]. Utzolino A., Bluhm K. Die Synthese und Kristallstruktur von $Ba_2Mn\ (B_3O_6)_2$ und $Ba_2Co\ (B_3O_6)_2$/Synthesis and Crystal Structure of $Ba_2Mn\ (B_3O_6)_2$ and $Ba_2Co\ (B_3O_6)_2$ //Zeitschrift für Naturforschung B. – 1996. – T. 51. – №. 7. – C. 907-911.

[10]. Stenger, C. G. F., G. C. Verschoor, and D. J. W. Ijdo. "The crystal structure of $Ni_5TiB_2O_{10}$." *Materials Research Bulletin* 8.11 (1973): 1285-1292.

[11]. Neuendorf, H., and W. Gunsser. "Transition from quasi one dimensional to spin glass behaviour in insulating $Fe_xGa_{1-x}MgBO_4$." *Journal of magnetism and magnetic materials* 151.1-2 (1995): 305-313.

[12]. Hriljac, J. A., et al. "The synthesis and crystal structures of the related series of aluminoborates: $Co_{2.1}Al_{0.9}BO_5$, Ni_2AlBO_5, and Cu_2AlBO_5." *Journal of Solid State Chemistry* 84.2 (1990): 289-298.

[13]. Cooper, J. J., and R. J. D. Tilley. "An electron microscope and X-ray diffraction study of some synthetic $(Mg, Mn)_3BO_5$ oxyborates." *Journal of Solid State Chemistry* 97.2 (1992): 452-465.

[14]. Cai, G. M., et al. "Subsolidus phase relations in $CoO–In_2O_3–B_2O_3$ system and crystal structure of $Co_{3-X}In_XBO_5$ solid solution for $0< X\leqslant 1$." *Journal of Alloys and Compounds* 615 (2014): 809-816.

[15]. Bluhm, K., and Hh Müller-Buschbaum. "Oxometallate mit inselförmigen boreinlagerungen $Ni_5MB_2O_{10}$." *Journal of the Less Common Metals* 147.1 (1989): 133-139.

[16]. Bluhm, K., and Hk Müller-Buschbaum. "Zur Stabilisierung der Oxidationsstufe M^{IV} im $Ni_5MB_2O_{10}$-Typ." *Zeitschrift für anorganische und allgemeine Chemie* 579.1 (1989): 111-115.

[17]. Bertaut, E. F. "Structures des boroferrites." *Acta Crystallographica* 3.6 (1950): 473-474.

[18]. Wilson A. J. C. (ed.). "International Tables for Crystallography: Mathematical, physical, and chemical tables." *International Union of Crystallography*, (1992). Vol. 3.

[19]. Takeuchi, Y., Takéo Watanabe, and T. Ito. "The crystal structures of warwickite, ludwigite and pinakiolite." *Acta Crystallographica* 3.2 (1950): 98-107.

[20]. Bovin, J-O., M. O'Keeffe, and M. A. O'Keefe. "Electron microscopy of oxyborates. I. Defect structures in the minerals pinakiolite, ludwigite, orthopinakiolite and takéuchiite." *Acta Crystallographica Section A: Crystal Physics, Diffraction, Theoretical and General Crystallography* 37.1 (1981): 28-35.

[21]. Kravchuk T. A, Nekrasov I. Ya. Grigor'ev A.P. *Zapiski Vsesouznogo mineralogicheskogo obshchestva*. (1966). 272. (in Russian).

[22]. Wood, Richard M., and Gus J. Palenik. "Bond valence sums in coordination chemistry. A simple method for calculating the oxidation state of cobalt in complexes containing only Co− O bonds." *Inorganic chemistry* 37.16 (1998): 4149-4151.

[23]. Palenik G. J. "Bond Valence Sums in Coordination Chemistry Using Oxidation State Independent R_0 Values. A Simple Method for Calculating the Oxidation State of Manganese in Complexes Containing Only Mn-O Bonds". *Inorganic chemistry*. 36.21 (1997). 4888-4890.

[24]. Urusov, V. S., and I. P. Orlov. "State-of-art and perspectives of the bond-valence model in inorganic crystal chemistry." *CRYSTALLOGRAPHY REPORTS C/C OF KRISTALLOGRAFIIA* 44 (1999): 686-709.

[25]. Sánchez, D. R., et al. "Magnetism and charge ordering in $Fe3O_2BO_3$ studied by Fe^{57} Mössbauer spectroscopy." *Physical Review B* 70.17 (2004): 174452.

[26]. Douvalis, A. P., et al. "Mössbauer and magnetization studies of Fe_3BO_5." *Journal of Physics: Condensed Matter* 14.12 (2002): 3303.

[27]. Attfield, J. Paul, John F. Clarke, and David A. Perkins. "Magnetic and crystal structures of iron borates." *Physica B: Condensed Matter* 180 (1992): 581-584.

[28]. Bordet, Pierre, and Emmanuelle Suard. "Magnetic structure and charge ordering in Fe_3BO_5: A single-crystal x-ray and neutron powder diffraction study." *Physical Review B* 79.14 (2009): 144408.

[29]. Freitas, D. C., et al. "Partial magnetic ordering and crystal structure of the ludwigites $Co_2FeO_2BO_3$ and $Ni_2FeO_2BO_3$." *Physical Review B* 79.13 (2009): 134437.

[30]. Guimaraes, R. B., et al. "Cation-mediated interaction and weak ferromagnetism in $Fe_3O_2BO_3$." *Physical Review B* 60.9 (1999): 6617.

[31]. Fernandes, J. C., et al. "Specific heat of $Fe_3O_2BO_3$: Evidence for a Wigner glass phase." *Physical Review B* 61.2 (2000): R850.

[32]. Kazak, N. V., et al. "Conductivity study of $Co_3O_2BO_3$ and $Co_{3-x}Fe_xO_2BO_3$ oxyborates." *Solid State Phenomena*. Vol. 152. Trans Tech Publications, 2009.

[33]. Ivanova, N. B., et al. "Crystal structure and magnetic anisotropy of ludwigite $Co_2FeO_2BO_3$." *Journal of Experimental and Theoretical Physics* 113.6 (2011): 1015-1024.

[34]. Freitas, D. C., et al. "Structural and magnetic properties of the oxyborate Co_5Ti $(O_2BO_3)2$." *Physical Review B* 81.2 (2010): 024432.

[35]. Neuendorf, H., and W. Gunβer. "Transition from quasi-one-dimensional to spin-glass behaviour in insulating $FeMg_2BO_5$." *Journal of magnetism and magnetic materials* 173.1-2 (1997): 117-125.

[36]. Petrakovskiĭ, G. A., et al. "Magnetic properties of single crystals of ludwigites Cu_2MBO_5 (M= Fe^{3+}, Ga^{3+})." *Physics of the Solid State* 51.10 (2009): 2077-2083.

[37]. Vallejo, E., and M. Avignon. "Spin and charge ordering in three-leg ladders in oxyborates." *Physical review letters* 97.21 (2006): 217203.

[38]. Vallejo, E., and M. Avignon. "Spin ordering in three-leg ladders in Ludwigite systems." *Journal of Magnetism and Magnetic Materials* 310.2 (2007): 1130-1132.

[39]. Vallejo, E., et al. "Magnetic polaron structures in the one-dimensional double and super-exchange model." *Solid State Communications* 149.3 (2009): 126-130.

[40]. Vallejo, E. "Magnetoelastic effect in an exchange model." *Journal of Magnetism and Magnetic Materials* 321.6 (2009): 640-643.

[41]. Anisimov, Vladimir I., F. Aryasetiawan, and A. I. Lichtenstein. "First-principles calculations of the electronic structure and spectra of strongly correlated systems: the LDA+ U method." *Journal of Physics: Condensed Matter* 9.4 (1997): 767.

[42]. Liechtenstein, A. I., V. I. Anisimov, and J. Zaanen. "Density-functional theory and strong interactions: Orbital ordering in Mott-Hubbard insulators." *Physical Review B* 52.8 (1995): R5467.

[43]. Whangbo, M-H., et al. "Theoretical investigation of the spin exchange interactions and magnetic properties of the homometallic ludwigite $Fe_3O_2BO_3$." *Inorganic chemistry* 41.8 (2002): 2193-2201.

[44]. Hirsch, Jorge E., and Jorge V. José. "Singular thermodynamic properties in random magnetic chains." *Physical Review B* 22.11 (1980): 5339.

[45]. Matos, M., et al. "First principles calculation of magnetic order in a low-temperature phase of the iron ludwigite." *Journal of Magnetism and Magnetic Materials* 374 (2015): 148-152.

[46]. Krupička, Svatopluk. "Erratum to: Allgemeine Grundlagen." *Physik der Ferrite und der verwandten magnetischen Oxide*. Vieweg+ Teubner Verlag, 1973. 781-781.

[47]. Anderson, Philip W. "Theory of magnetic exchange interactions: exchange in insulators and semiconductors." *Solid state physics* 14 (1963): 99-214.

[48]. Van Gorkom G. GP., Henning J. C. M., Stapele R. F. "Optical spectra of Cr^{3+} pairs in the spinel $ZnGa_2O_4$" *Physical Review*. B 8.3 (1974). 955-973

[49]. Weakliem, Herbert A. "Optical spectra of Ni2+, Co2+, and Cu2+ in tetrahedral sites in crystals." *The Journal of Chemical Physics* 36.8 (1962): 2117-2140.

[50]. Eremin, M. V. "Theory of exchange interaction of magnetic ions in dielectrics." *Spectroscopy of Crystals* (1985): 150-172.

[51]. Bayukov, O. A., and A. F. Savitskii. "The magnetic properties of dielectrics can be predicted." *Physics of the Solid State* 36 (1994): 1049-1057.

[52]. Bayukov, O. A., and A. F. Savitskii. "The Prognostication Possibility of Some Magnetic Properties for Dielectrics on the Basis of Covalency Parameters of Ligand-Cation Bonds." *physica status solidi (b)* 155.1 (1989): 249-255.

[53]. Ivanova, N. B., et al. "Magnetic and electrical properties of cobalt oxyborate Co_3BO_5." *Physics of the Solid State* 49.4 (2007): 651-653.

[54]. Freitas, D. C., et al. "Structure and magnetism of homometallic ludwigites: $Co_3O_2BO_3$ versus $Fe_3O_2BO_3$." *Physical Review B* 77.18 (2008): 184422.

[55]. Norrestam, R., et al. "Structural investigation of two synthetic oxyborates: the mixed magnesium-manganese and the pure cobalt ludwigites, $Mg_{1.93(2)}Mn_{1.07(2)}O_2BO_3$ and $Co_3O_2BO_3$." *Zeitschrift für Kristallographie-Crystalline Materials* 189.1-4 (1989): 33-42.

[56]. Shannon, Robert D. "Revised effective ionic radii and systematic studies of interatomic distances in halides and chalcogenides." *Acta crystallographica section A: crystal physics, diffraction, theoretical and general crystallography* 32.5 (1976): 751-767.

[57]. Kazak, N. V., et al. "Crystal and local atomic structure of $MgFeBO_4$, $Mg_{0.5}Co_{0.5}FeBO_4$ and $CoFeBO_4$: Effects of Co substitution." *physica status solidi (b)* 252.10 (2015): 2245-2258.

[58]. Z.-X.Huang, W.-D.Cheng and H. Zhang. "Synthesis and Crystal Structure of Borate Oxide Co_3BO_5" Chin. J. Struct. Chem. 20.2 (2001). 97-99.

[59]. Mir, Mt, et al. "Structural Transition and Pair Formation in $Fe_3O_2BO_3$." *Physical review letters* 87.14 (2001): 147201.

[60]. E. Kondorsky. *Physik. Z. Sowjetunion*. 11 (1937). 597

[61]. Chikazumi, Sōshin. *Physics of magnetism*. Wiley, 1964.

[62]. Ropka, Z., and R. J. Radwanski. "5 D term origin of the excited triplet in $LaCoO_3$." *Physical Review B* 67.17 (2003): 172401.

[63]. Trukhanov, S. V., A. V. Trukhanov, and H. Szymczak. "Effect of magnetic fields on magnetic phase separation in anion-deficient manganite $La_{0.70}Sr_{0.30}MnO_{2.85}$." *Low temperature physics* 37.6 (2011): 465-469.

[64]. Bayukov O. A., SavitskiiA. "*Indirect exchange in ferrites - spinels*". – Krasnoyarsk. L. V. Kirensky Institute of Physics. (1989). 61 (in Russian).

[65]. NazarenkoI.I, SofronovaS.N. "*Group-theoretical analysis of possible magnetic structures of a solid solution* $Ni_5GeO_4(BO_3)_2$." Bulletin of the M.F. Reshetnev Siberian State Aerospace University. 1.47. (2013). 63 – 67.(in Russian).

APPENDIX

Atomic coordinates for $Co_{2,25}Fe_{0,75}O_2BO_3$

	x/a	*y/b*	*z/c*
Co1	0.50000	0.50000	0.00000
Co2	0.00000	0.50000	0.50000
Co3	0.50069	0.22057	0.00000
Co4	0.26212	0.38440	0.50000
Fe4	0.39309	0.35669	0.00000
O1	0.37594	0.13979	0.50000
O2	0.15475	0.23677	0.50000
O3	0.11506	0.42270	0.00000
O4	0.34734	0.54210	0.50000
O5	0.50000	0.50000	0.00000
B	0.22468	0.13861	0.50000

Atomic coordinates for $Co_{1,7}Mn_{1,3}O_2BO_3$

	x/a	*y/b*	*z/c*	*SOF*	*U*(*eq*)
Co1	0.50000	0.50000	0.00000	0.17416	0.00613
Mn1	0.50000	0.50000	0.00000	0.07584	0.00613
Co2	0.00000	0.50000	0.50000	0.17379	0.00662
Mn2	0.00000	0.50000	0.50000	0.07621	0.00662
Co3	-0.00182	0.27888	0.00000	0.33253	0.00630
Mn3	-0.00182	0.27888	0.00000	0.16747	0.00630
Co4	0.26016	0.38426	0.50000	0.17557	0.00566
Mn4	0.26016	0.38426	0.50000	0.32443	0.00566
O1	-0.10731	0.14281	0.00000	0.50000	0.01253
O2	0.12586	0.64094	0.50000	0.50000	0.00992
O3	0.34996	0.54236	0.50000	0.50000	0.01044
O4	0.14948	0.23574	0.50000	0.50000	0.01147
O5	0.11387	0.42005	0.00000	0.50000	0.01489
B	0.22468	0.13861	0.50000	0.50000	0.00855

Atomic coordinates$Co_{2,88}Cu_{0,12}O_2BO_3$

	x/a	*y/b*	*z/c*	*SOF*	*U*(*eq*)
Co1	0.00000	0.00000	0.00000	0.25000	0.00593
Co2	0.50000	0.00000	0.50000	0.25000	0.00577
Co3	-0.00444	0.27680	0.00000	0.50000	0.00565
Co4	0.24089	0.11307	0.50000	0.43930	0.00470
Cu4	0.24089	0.11307	0.50000	0.06070	0.00470
O1	0.11292	0.14216	0.00000	0.50000	0.00852
O2	-0.12177	0.42118	0.00000	0.50000	0.01183
O3	-0.16286	0.23883	0.50000	0.50000	0.00907
O4	0.15797	-0.03939	0.50000	0.50000	0.01106
O5	0.11674	0.36164	0.50000	0.50000	0.01279
B	0.26417	0.36226	0.50000	0.50000	0.00374